Eur. Phys. J. C (2024) 84:257
https://doi.org/10.1140/epjc/s10052-024-12585-0

THE EUROPEAN PHYSICAL JOURNAL C

Regular Article - Theoretical Physics

Extended gravitational vortex without dark matter

G. O. Ludwig[1,2,a]

[1] National Institute for Space Research, São José dos Campos, SP 12227-010, Brazil
[2] National Commission for Nuclear Energy, Rio de Janeiro, RJ 22294-900, Brazil

Received: 3 January 2024 / Accepted: 18 February 2024

Abstract This paper analyzes, within the extended gravitoelectromagnetic (GEM) formulation, the equilibrium of a large scale gravitational system formed by rotating dust. The force balance equation gives the rotation velocity in terms of the GEM fields. Boundary conditions for the fields are introduced using Helmholtz's decomposition and the virtual casing principle. Hydro-gravitomagnetic Cauchy invariance is implemented to relate the fluid and gravitomagnetic field vorticities. An energy conservation equation gives the rotation velocity in terms of the gravitational field and respective boundary values. A detailed solution is calculated for the case of rotating oblate spheroids. The equilibrium is in the form of a sheared rotational vortex, without introducing dark matter. The results are consistent with the Tully–Fisher relation and the Virginia Trimble correlations.

1 Introduction

For more than a century the study of large scale gravitational systems encountered many phenomena that could not be explained by Newtonian gravity. These studies include the work on galaxy clusters pioneered by Zwicky [1–5], and the detailed observation of the rotation curve of galaxies by Rubin and many others [6–10]. Recently, the rotation of globular and galaxy clusters has been re-examined [11–15]. These studies are mostly observational. In fact, the straightforward application of Newtonian physics failed to explain the observations, leading to the introduction of the "dark matter" concept [16]. At the present time this concept is used to explain a variety of astrophysical observations, as well as to advance cosmological theories. Nevertheless, there is still no direct evidence of "dark matter" in nature, and its introduction in the models is artificial.

First attempts to use General Relativity (GR) in modeling galaxies refer to the works by Cooperstock and Tieu [17], and Balasin and Grumiller [18]. The Cooperstock and Tieu model was used by Magalhães and Cooperstock to estimate the mass density and size of spiral galaxies [19], while the Balasin an Grumiller rigid model was later generalized by Astesiano et al. [20] to differentially rotating dust. Purely geometric aspects of GR in the galactic dynamics were also considered by Astesiano and Ruggiero [21]. The scope of these studies is limited by the difficulty in obtaining realistic models to galaxies in the context of GR. One must point out that extended gravity theories can also be set about to deal with the dark matter problem. In fact, expected improvements in the angular and frequency dependent response of interferometric gravitational wave detectors may eventually discern which of the proposed theories holds true compared with General Relativity, as discussed by Corda [22].

A practical model of galactic dynamics was developed by the author [23] using an extended gravitoelectromagnetic (GEM) theory [24,25]. This theory reproduced the galactic rotation curves of diverse galaxies without need for dark matter. The results of the GEM theory were confirmed by Srivastava et al. [26] using a stationary, axially-symmetric Weyl metric in the weak-field limit (this formalism is equivalent to the GEM approach). Clearly, the failure of Newtonian theory in explaining the dynamics of extended astrophysical objects derives from the neglect of mass currents and associated gravitomagnetic (GM) field effects. Ironically, mass current effects were introduced by Heaviside [27] in his elegant analogy between gravitational and electromagnetic theories, before the advent of special relativity.

It is now well established that gravitomagnetic effects have an important role in understanding the dynamics of extended gravitationally confined systems, as pointed out by Ruggiero, Ortolan and Speake [28], and by Astesiano and Ruggiero [29]. One must also point out that, contrary to many objections and questions concerning the form of the Lorentz-like

[a] e-mail: gerson.ludwig@inpe.br (corresponding author)

Published online: 11 March 2024

term of the geodesic equation, as discussed by Ruggiero [30], the extended gravitoelectromagnetic theory is not limited to slow-motion, weak relativistic effects. In fact, the simplest form of the theory is valid to all orders in c^{-1} [24]. Only the space-space components of the metric tensor are initially neglected according to the weak-field approximation, but even these terms can be reinstated to order G^2. The form of the Lorentz-like term depends, essentially, if the fluid and test particle motions are both, either, or neither relativistic [25].

Recently, the author examined the rotational equilibrium of globular and galaxy clusters in the gravitomagnetic context. The flowing dust was considered in sedimentation equilibrium in the gravitational field. Presumably, the stars in a large system are in free-fall motion described by the balance between the centrally directed collective gravitational attraction, the latitudinal outward centrifugal force, and the skew Lorentz force (Coriolis effect). The results were promising, but did not give a self-consistent result without proper boundary conditions at the fluid-vacuum interface [31]. The present paper deals with the same problem more precisely, introducing suitable boundary conditions.

The paper is organized as follows. Section 2 lists the GEM equations of motion for a weakly relativistic perfect fluid. Assuming stationary conditions with azimuthal symmetry, the equations can be reduced to a field equation linking the scalar gravitational potential to the flux function of the gravitomagnetic field (the pressure modifies the scalar potential, but is neglected in the case of fluid dust). The field equation is complemented by Gauss's law for the scalar potential and Ampère's law for the flux function. The rotation velocity is determined by the force balance equation. Section 3 introduces the boundary conditions for the field equation in terms of a Helmholtz decomposition. The volume and surface integrals in the decomposition correspond to the particular and homogeneous solutions, respectively. Equivalent surface mass and mass current densities are defined in terms of the field components just outside the fluid-vacuum interface. In the vacuum region the fields are represented by sums over multipole components, determining the form of the surface densities in terms of the external multipoles. The zero-order multipole components define the character of the solution. In the present paper it is assumed that the scalar potential vanishes at infinity, while the flux function remains constant, defining one class of rotational vortices. According to the virtual casing principle the particular solutions are linked to the multipole expansions of the external GEM field at the fluid-vacuum interface, while the homogeneous solutions are given in terms of surface integrals over the surface densities, also linked to the same multipole expansions. Together with the Maxwell source equations, the force balance equation gives the final link between the internal GE and GM fields. Then, in Sect. 4 the set of nonlinear integro-differential equations for the GEM field is simplified introducing the hydro-gravitomagnetic Cauchy invariance, which leads to the energy conservation equation in the rotating fluid in terms of the boundary conditions. Section 5 specializes the previous equations to the case of rotating oblate spheroids, discussing the two classes of fixed- and free-boundary problems. It is shown how the rotation velocity at the fluid-vacuum interface is determined in terms of the equivalent surface current densities in order to give finite values to the surface integrals defining the homogeneous solutions. It is also demonstrated how the force balance condition leads to a constraint in the mass density profile while linking the fluid velocity at the equatorial edge to sums of multipole coefficients. In Sect. 6 the rotation velocity at the equatorial edge and the total mechanical angular momentum are estimated assuming a mass distribution over a relativistic ring. It is shown that this crude approximation gives results consistent with the Tully–Fisher relation and the Virginia Trimble correlations. Finally, in Sect. 7 a monotonic Gaussian mass density profile is implemented to tentatively describe the full equilibrium of very large rotating gravitational systems. The equilibrium solution is determined in the form of a rotational vortex with shear. Section 8 gives the final comments and conclusions of the work.

2 Dynamics of rotating fluid

According to the extended gravitoelectromagnetic (GEM) theory in its weakly relativistic formulation [24], the rotating fluid dynamics is described by the equation of continuity

$$\frac{\partial \rho}{\partial t} + \nabla \cdot (\rho \boldsymbol{u}) = 0, \tag{2.1}$$

the momentum density conservation equation

$$\frac{\partial}{\partial t}(\rho \boldsymbol{u}) + \nabla \cdot (\rho \boldsymbol{u}\boldsymbol{u}) = -\nabla p + \rho \boldsymbol{E} + \boldsymbol{j} \times \boldsymbol{B}, \tag{2.2}$$

the Maxwell source equations

$$\begin{cases} \nabla \cdot \boldsymbol{E} &= -4\pi G\rho & \text{GE Gauss's law} \\ \nabla \times \boldsymbol{B} &= -\dfrac{4\pi G}{c^2}\boldsymbol{j} + \dfrac{1}{c^2}\dfrac{\partial \boldsymbol{E}}{\partial t} & \text{GEM Ampère's law} \\ \nabla \cdot \boldsymbol{B} &= 0 & \text{GM Gauss's law} \end{cases} \tag{2.3}$$

and an equation of state for the fluid pressure p. The mass current density $\boldsymbol{j} = \rho \boldsymbol{u}$ is given in terms of the mass density ρ and the fluid velocity $\boldsymbol{u}$. The gravitoelectric (GE) field $\boldsymbol{E}$ and the gravitomagnetic (GM) field $\boldsymbol{B}$ are given in terms of the potentials ϕ and $\boldsymbol{A}$:

$$\begin{cases} \boldsymbol{E} = -\nabla\phi - \dfrac{\partial \boldsymbol{A}}{\partial t} \\ \boldsymbol{B} = \nabla \times \boldsymbol{A} \end{cases} \tag{2.4}$$

In this way, the motion is described by nine equations in the five perfect fluid variables ρ, $\boldsymbol{u}$, and p, plus the four gravitoelectromagnetic field variables ϕ and $\boldsymbol{A}$. The fluid pressure is related to the mass density by an equation of state, and the redundant degree of freedom in the gravitomagnetic potentials is removed by an additional gauge condition, reducing the problem to seven equations in seven variables.

The momentum conservation equation for stationary flow ($\partial/\partial t \equiv 0$) can be written in terms of the potentials as

$$\rho \boldsymbol{u} \cdot (\nabla \boldsymbol{u}) = -\nabla p - \rho \nabla \phi + \boldsymbol{j} \times (\nabla \times \boldsymbol{A}) . \tag{2.5}$$

Assuming azimuthal symmetry ($\partial/\partial\varphi \equiv 0$), the fluid velocity and the vector potential have single components $\boldsymbol{u} = u_\varphi (r, \theta) \widehat{\boldsymbol{\varphi}}$ and $\boldsymbol{A} = A_\varphi (r, \theta) \widehat{\boldsymbol{\varphi}}$, respectively, in spherical polar coordinates (r, θ, φ). Here, $\widehat{\boldsymbol{\varphi}}$ is the unit vector in the azimuthal direction. Introducing the gravitomagnetic flux function $\psi (r, \theta) = r \sin\theta A_\varphi (r, \theta)$, the poloidal equilibrium equation becomes

$$\boldsymbol{F}_i (r, \theta) = -\nabla p (r, \theta) + \boldsymbol{F}_e (r, \theta) + \boldsymbol{F}_m (r, \theta) , \tag{2.6}$$

where $\boldsymbol{F}_i$, $\boldsymbol{F}_e$ and $\boldsymbol{F}_m$ represent the inertial, gravitoelectric and gravitomagnetic force densities, respectively,

$$\begin{cases} \boldsymbol{F}_i (r, \theta) &= -\dfrac{\rho (r, \theta) u_\varphi^2 (r, \theta)}{r} \left(\widehat{\boldsymbol{r}} + \cot\theta \widehat{\boldsymbol{\theta}} \right) \\ \boldsymbol{F}_e (r, \theta) &= \rho (r, \theta) \boldsymbol{E} = -\rho (r, \theta) \nabla \phi (r, \theta) \\ \boldsymbol{F}_m (r, \theta) &= j_\varphi (r, \theta) \widehat{\boldsymbol{\varphi}} \times \boldsymbol{B} = \dfrac{j_\varphi (r, \theta)}{r \sin\theta} \nabla \psi (r, \theta) \end{cases} \tag{2.7}$$

The curl of the unit vector $\widehat{\boldsymbol{\varphi}}$ forms an oblique projector

$$r \nabla \times \widehat{\boldsymbol{\varphi}} = \cot\theta \widehat{\boldsymbol{r}} - \widehat{\boldsymbol{\theta}}, \tag{2.8}$$

which, upon application on the equilibrium equation (2.6), cancels the inertial term giving an equation for the geodesic path of a fluid element

$$r (\nabla \times \widehat{\boldsymbol{\varphi}}) \cdot \left(-\nabla p (r, \theta) - \rho (r, \theta) \nabla \phi (r, \theta) + \frac{j_\varphi (r, \theta)}{r \sin\theta} \nabla \psi (r, \theta) \right) = 0. \tag{2.9}$$

The free-fall condition (2.9) is a skew combination of the radial and polar equilibrium equations:

$$\begin{cases} -\rho (r, \theta) u_\varphi^2 (r, \theta) &= -r \dfrac{\partial p (r, \theta)}{\partial r} - \rho (r, \theta) r \dfrac{\partial \phi (r, \theta)}{\partial r} + \dfrac{j_\varphi (r, \theta)}{r \sin\theta} r \dfrac{\partial \psi (r, \theta)}{\partial r} & \text{radial equilibrium} \\ -\rho (r, \theta) u_\varphi^2 (r, \theta) \cot\theta &= -\dfrac{\partial p (r, \theta)}{\partial \theta} - \rho (r, \theta) \dfrac{\partial \phi (r, \theta)}{\partial \theta} + \dfrac{j_\varphi (r, \theta)}{r \sin\theta} \dfrac{\partial \psi (r, \theta)}{\partial \theta} & \text{polar equilibrium} \end{cases} \tag{2.10}$$

Assuming an equation of state in the polytropic form $p \propto \rho^{(\nu+1)/\nu}$, where ν is the constant polytropic index, the free-fall equation can be written in the simplified form

$$r (\nabla \times \widehat{\boldsymbol{\varphi}}) \cdot \left[-\nabla \left(\phi (r, \theta) + (\nu + 1) \frac{p (r, \theta)}{\rho (r, \theta)} \right) + \frac{u_\varphi (r, \theta)}{r \sin\theta} \nabla \psi (r, \theta) \right] = 0. \tag{2.11}$$

For vanishing rotation ($u_\varphi = 0$) the oblique force balance equation reduces to hydrostatic equilibrium, giving

$$\phi = -\frac{(\nu + 1) p_0}{\rho_0} \left(\frac{\rho}{\rho_0} \right)^{1/\nu} , \tag{2.12}$$

where p_0 and ρ_0 denote a reference state. Combined with the gravitoelectric Poisson equation $\nabla^2 \phi = 4\pi G\rho$, this leads to the nonlinear Lane–Emden equation for the gravitational potential ϕ of a polytropic fluid. The polytropic model can be used to describe the equilibrium of high-density compact objects [32–35], but is not adequate to describe the processes involved in low-density, extended collisionless astrophysical systems with effectively vanishing pressure $p \cong 0$. Nevertheless, assuming $\nu = 5$ the polytropic equilibrium was used by H.C. Plummer in 1915 as a mathematical model in the analysis of the mass density distribution in twelve (presumably static) clusters [36].

On the other hand, for a pressureless system ($p = 0$) the free-fall condition (2.9) reduces to

$$r (\nabla \times \widehat{\boldsymbol{\varphi}}) \cdot \left(-\rho (r, \theta) \nabla \phi (r, \theta) + \frac{j_\varphi (r, \theta)}{r \sin\theta} \nabla \psi (r, \theta) \right) = 0. \tag{2.13}$$

Furthermore, the density $\rho (r, \theta)$ is given in terms of the scalar potential $\phi (r, \theta)$ by Gauss's law, and the current density $j_\varphi (r, \theta)$ is given in terms of the flux function $\psi (r, \theta)$ by Ampère's law

$$\begin{cases} \rho (r, \theta) &= \dfrac{\nabla^2 \phi (r, \theta)}{4\pi G} & \text{Gauss's law} \\ j_\varphi (r, \theta) &= \dfrac{c^2 r \sin\theta}{4\pi G} \nabla \cdot \left(\dfrac{\nabla \psi (r, \theta)}{r^2 \sin^2\theta} \right) & \text{Ampère's law} \end{cases} \tag{2.14}$$

Hence, for vanishing pressure the free-fall condition (2.9) gives a nonlinear, third-order partial differential equation relating the GE scalar potential $\phi (r, \theta)$ and the GM flux function $\psi(r, \theta)$

$$\nabla \cdot \left(\frac{\nabla \phi (r, \theta)}{c^2} \right) (\nabla \times \widehat{\boldsymbol{\varphi}}) \cdot \nabla \phi (r, \theta) = \nabla \cdot \left(\frac{\nabla \psi (r, \theta)}{r^2 \sin^2\theta} \right) (\nabla \times \widehat{\boldsymbol{\varphi}}) \cdot \nabla \psi (r, \theta) . \tag{2.15}$$

The field equation (2.15) relates ϕ to ψ (and vice-versa), while the source equations (2.14) determine the mass dis-

tribution and the mass motion in the gravitoelectromagnetic field, describing the local exchange of energy and momentum between the gravitational field and matter. Finally, the radial equilibrium equation (2.10) gives a quadratic equation for the fluid velocity $u_\varphi(r,\theta)$ in terms of the radial derivatives of the GEM fields

$$u_\varphi^2(r,\theta)+\frac{u_\varphi(r,\theta)}{\sin\theta}\frac{\partial\psi(r,\theta)}{\partial r}-r\frac{\partial\phi(r,\theta)}{\partial r}=0. \tag{2.16}$$

The polar equilibrium equation (2.10) gives an additional quadratic equation for the fluid velocity $u_\varphi(r,\theta)$ in terms of the polar derivatives of the GEM fields

$$u_\varphi^2(r,\theta)+\frac{u_\varphi(r,\theta)}{r\cos\theta}\frac{\partial\psi(r,\theta)}{\partial\theta}-\tan\theta\frac{\partial\phi(r,\theta)}{\partial\theta}=0. \tag{2.17}$$

Eliminating $u_\varphi(r,\theta)$ in Eqs. (2.16) and (2.17) gives an alternative differential relation between the GEM fields $\psi(r,\theta)$ and $\phi(r,\theta)$. Moreover, the equivalence of these equations gives

$$u_\varphi(r,\theta)=r\sin\theta\left(\frac{r\partial\phi/\partial r-\tan\theta\partial\phi/\partial\theta}{r\partial\psi/\partial r-\tan\theta\partial\psi/\partial\theta}\right). \tag{2.18}$$

Polar equilibrium in a pressureless system is not possible without taking into account the equivalent Larmor gravitomagnetic field $\boldsymbol{B}$ in the rotating frame [37].

Assuming symmetry with respect to the equatorial plane $\theta=\pi/2$ the field equation (2.15) can be put in a convenient symmetric form by defining the potential operator $\Phi[\phi(r,\theta)]$

$$\begin{aligned}\Phi[\phi(r,\theta)]&=r^6\sin^2\theta\tan\theta\nabla\cdot\left(\frac{\nabla\phi(r,\theta)}{c^2}\right)(\nabla\times\widehat{\boldsymbol{\varphi}})\cdot\nabla\phi(r,\theta)\\&=\frac{4\pi G}{c^2}r^6\sin^2\theta\tan\theta\rho(r,\theta)(\nabla\times\widehat{\boldsymbol{\varphi}})\cdot\nabla\phi(r,\theta)\\&=\frac{r^2\sin^2\theta}{c^2}\left[\frac{\partial}{\partial r}\left(r^2\frac{\partial\phi(r,\theta)}{\partial r}\right)+\frac{1}{\sin\theta}\frac{\partial}{\partial\theta}\right.\\&\quad\left.\times\left(\sin\theta\frac{\partial\phi(r,\theta)}{\partial\theta}\right)\right]\\&\quad\times\left(r\frac{\partial\phi(r,\theta)}{\partial r}-\tan\theta\frac{\partial\phi(r,\theta)}{\partial\theta}\right).\end{aligned} \tag{2.19}$$

and the flux operator $\Psi[\psi(r,\theta)]$

$$\begin{aligned}\Psi[\psi(r,\theta)]&=r^6\sin^2\theta\tan\theta\nabla\cdot\left(\frac{\nabla\psi(r,\theta)}{r^2\sin^2\theta}\right)(\nabla\times\widehat{\boldsymbol{\varphi}})\\&\quad\cdot\nabla\psi(r,\theta)\\&=\frac{4\pi G}{c^2}r^5\sin\theta\tan\theta j_\varphi(r,\theta)(\nabla\times\widehat{\boldsymbol{\varphi}})\cdot\nabla\psi(r,\theta)\\&=\left[r^2\frac{\partial^2\psi(r,\theta)}{\partial r^2}+\sin\theta\frac{\partial}{\partial\theta}\left(\frac{1}{\sin\theta}\frac{\partial\psi(r,\theta)}{\partial\theta}\right)\right]\\&\quad\times\left(r\frac{\partial\psi(r,\theta)}{\partial r}-\tan\theta\frac{\partial\psi(r,\theta)}{\partial\theta}\right).\end{aligned} \tag{2.20}$$

The flux operator (2.20) is the product of the Grad-Shafranov operator for $\psi(r,\theta)$ by the projected oblique component of the rotated gravitomagnetic field. Although this is not evident at this point, the Grad-Shafranov term corresponds to the particular solution of the flux function $\psi(r,\theta)$, while the oblique field term corresponds to the full gravitomagnetic field, which is formed by the sum of the particular and homogeneous solutions. The same argument is true for the scalar potential $\phi(r,\theta)$, with the Gauss term in the potential operator (2.19) corresponding to the particular solution and the oblique term corresponding to the full field solution. This topic will be clarified at the end of Sect. 3. Nevertheless, solutions of the field equation $\Phi[\phi(r,\theta)]=\Psi[\psi(r,\theta)]$ with appropriate boundary conditions determine the rotating fluid mass density and mass current density by means of the source equations (2.14). The boundary conditions issue is addressed in the next section.

3 Boundary conditions

According to Helmholtz's theorem for stationary problems ($\partial/\partial t\equiv 0$) in a three-dimensional region V, the combined gravitoelectromagnetic field $\boldsymbol{H}=\boldsymbol{E}+c\boldsymbol{B}$ can be decomposed into an irrotational component and a solenoidal component

$$\boldsymbol{H}=-\nabla\phi+c\nabla\times\boldsymbol{A} \tag{3.1}$$

so that

$$\begin{cases}\phi(\boldsymbol{r})=\dfrac{1}{4\pi}\displaystyle\int_V\frac{\nabla'\cdot\boldsymbol{H}(\boldsymbol{r}')}{|\boldsymbol{r}-\boldsymbol{r}'|}dV'-\frac{1}{4\pi}\oint_S\frac{\widehat{\boldsymbol{n}}'\cdot\boldsymbol{H}(\boldsymbol{r}')}{|\boldsymbol{r}-\boldsymbol{r}'|}dS'\\ \boldsymbol{A}(\boldsymbol{r})=\dfrac{1}{4\pi c}\displaystyle\int_V\frac{\nabla'\times\boldsymbol{H}(\boldsymbol{r}')}{|\boldsymbol{r}-\boldsymbol{r}'|}dV'-\frac{1}{4\pi c}\oint_S\frac{\widehat{\boldsymbol{n}}'\times\boldsymbol{H}(\boldsymbol{r}')}{|\boldsymbol{r}-\boldsymbol{r}'|}dS'\end{cases} \tag{3.2}$$

where S is the surface that encloses the volume V and $\widehat{\boldsymbol{n}}$ is the outward unit vector normal to the surface S. The source density is $D=\nabla\cdot\boldsymbol{H}=-\nabla^2\phi=-4\pi G\rho$ and the circulation density is $\boldsymbol{C}=\nabla\times\boldsymbol{H}=c\nabla\times(\nabla\times\boldsymbol{A})=-(4\pi G/c)\boldsymbol{j}$. It follows that

$$\begin{cases}\phi(\boldsymbol{r})=-G\displaystyle\int_V\frac{\rho(\boldsymbol{r}')}{|\boldsymbol{r}-\boldsymbol{r}'|}dV'-\frac{1}{4\pi}\\ \qquad\times\displaystyle\oint_S\widehat{\boldsymbol{n}}'\cdot\frac{\boldsymbol{E}(\boldsymbol{r}')+c\boldsymbol{B}(\boldsymbol{r}')}{|\boldsymbol{r}-\boldsymbol{r}'|}dS'\\ \boldsymbol{A}(\boldsymbol{r})=-\dfrac{G}{c^2}\displaystyle\int_V\frac{\boldsymbol{j}(\boldsymbol{r}')}{|\boldsymbol{r}-\boldsymbol{r}'|}dV'-\frac{1}{4\pi c}\\ \qquad\times\displaystyle\oint_S\widehat{\boldsymbol{n}}'\times\frac{\boldsymbol{E}(\boldsymbol{r}')+c\boldsymbol{B}(\boldsymbol{r}')}{|\boldsymbol{r}-\boldsymbol{r}'|}dS'\end{cases} \tag{3.3}$$

At the fluid-vacuum interface the gravitoelectric and gravitomagnetic Gauss's laws give

$$\begin{cases}\nabla\cdot\boldsymbol{E}=-4\pi G\rho\Longrightarrow\widehat{\boldsymbol{n}}\cdot\langle\langle\boldsymbol{E}\rangle\rangle=-4\pi G\sigma_{\text{true}}\\ \nabla\cdot\boldsymbol{B}=0\qquad\Longrightarrow\widehat{\boldsymbol{n}}\cdot\langle\langle\boldsymbol{B}\rangle\rangle=0\end{cases} \tag{3.4}$$

where $\langle\langle\ldots\rangle\rangle$ denotes the increment across the interface and σ_{true} is the true surface mass density. Furthermore, in the

stationary state the laws of Faraday and Ampère give

$$\begin{cases} \nabla \times \boldsymbol{E} = 0 & \Longrightarrow \widehat{\boldsymbol{n}} \times \langle\langle \boldsymbol{E} \rangle\rangle = 0 \\ \nabla \times \boldsymbol{B} = -\dfrac{4\pi G}{c^2}\boldsymbol{j} & \Longrightarrow \widehat{\boldsymbol{n}} \times \langle\langle \boldsymbol{B} \rangle\rangle = -\dfrac{4\pi G}{c^2}\boldsymbol{K}_{\text{true}} \end{cases} \tag{3.5}$$

where $\boldsymbol{K}_{\text{true}}$ designates a true surface mass current density. The gravitoelectric field $\boldsymbol{E}$ and the gravitomagnetic field $\boldsymbol{B}$ are, respectively, normal and tangential to the fluid-vacuum interface. The combined field $\boldsymbol{H}$ has mixed components. Taking the gradient of ϕ and the curl of $\boldsymbol{A}$ and assuming that there are no true surface densities ($\sigma_{\text{true}} = 0$, $\boldsymbol{K}_{\text{true}} = 0$), the field $\boldsymbol{H}$ in the external region is given by

$$\begin{aligned} \boldsymbol{H}_{\text{ext}}(\boldsymbol{r}) &= -\frac{1}{4\pi}\oint_S \frac{\widehat{\boldsymbol{n}}' \cdot \boldsymbol{E}(\boldsymbol{r}')(\boldsymbol{r}-\boldsymbol{r}')}{|\boldsymbol{r}-\boldsymbol{r}'|^3} dS' \\ &\quad -\frac{c}{4\pi}\oint_S \frac{(\widehat{\boldsymbol{n}}' \times \boldsymbol{B}(\boldsymbol{r}')) \times (\boldsymbol{r}-\boldsymbol{r}')}{|\boldsymbol{r}-\boldsymbol{r}'|^3} dS', \end{aligned} \tag{3.6}$$

and in the internal region by

$$\begin{aligned} \boldsymbol{H}_{\text{int}}(\boldsymbol{r}) &= -G\int_V \frac{\rho(\boldsymbol{r}')(\boldsymbol{r}-\boldsymbol{r}')}{|\boldsymbol{r}-\boldsymbol{r}'|^3} dV' \\ &\quad -\frac{1}{4\pi}\oint_S \frac{\widehat{\boldsymbol{n}}' \cdot \boldsymbol{E}(\boldsymbol{r}')(\boldsymbol{r}-\boldsymbol{r}')}{|\boldsymbol{r}-\boldsymbol{r}'|^3} dS' \\ &\quad -\frac{G}{c^2}\int_V \frac{\boldsymbol{j}(\boldsymbol{r}') \times (\boldsymbol{r}-\boldsymbol{r}')}{|\boldsymbol{r}-\boldsymbol{r}'|^3} dV' \\ &\quad -\frac{c}{4\pi}\oint_S \frac{(\widehat{\boldsymbol{n}}' \times \boldsymbol{B}(\boldsymbol{r}')) \times (\boldsymbol{r}-\boldsymbol{r}')}{|\boldsymbol{r}-\boldsymbol{r}'|^3} dS'. \end{aligned} \tag{3.7}$$

The surface S plays the role of a virtual casing as formulated by Shafranov and Zakharov [38]. The virtual casing principle is related to the von Hagenow method [39–42]. A generalized virtual-casing principle was described by Hanson [43]. In general relativity the virtual casing corresponds to a boundary surface as originally defined by Israel [44].

Assuming azimuthal symmetry, the equivalent (fictitious) surface mass and surface mass current densities are defined at the surface S in terms of the normal component of $\boldsymbol{E}$ and of the tangential component of $\boldsymbol{B}$ just outside the fluid-vacuum interface by, respectively,

$$\begin{aligned} \sigma(r,\theta) &= -\frac{\widehat{\boldsymbol{n}} \cdot \boldsymbol{E}(r,\theta)}{4\pi G} \quad \text{and} \quad K_\varphi(r,\theta) \\ &= -\frac{c^2}{4\pi G}\,\widehat{\boldsymbol{n}} \times \boldsymbol{B}(r,\theta)|_\varphi\,, \end{aligned} \tag{3.8}$$

with $\widehat{\boldsymbol{n}}$ pointing outwards. In the present paper (r,θ,φ) forms a right-handed polar spherical coordinate system, but (r,θ) may equally well represent non-orthogonal coordinates in a right-handed (r,ζ,θ) axisymmetric system, with the toroidal angle variable $\zeta = -\varphi$. In whatever manner, the scalar potential and the flux function in the external region can be written in the form

$$\begin{cases} \phi_{\text{ext}}(r,\theta) = G\oint_S \dfrac{\sigma(r',\theta')}{|\boldsymbol{r}-\boldsymbol{r}'|} dS' \\ \psi_{\text{ext}}(r,\theta) = r\sin\theta \dfrac{G}{c^2}\oint_S \dfrac{K_\varphi(r',\theta')}{|\boldsymbol{r}-\boldsymbol{r}'|} dS' \end{cases} \tag{3.9}$$

and in the internal region V (with inverted signs for the surface sources since $\widehat{\boldsymbol{n}}$ is pointing inwards inside S)

$$\begin{cases} \phi_{\text{int}}(r,\theta) = -G\left(\displaystyle\int_V \frac{\rho(r',\theta')}{|\boldsymbol{r}-\boldsymbol{r}'|} dV' + \oint_S \frac{\sigma(r',\theta')}{|\boldsymbol{r}-\boldsymbol{r}'|} dS'\right) \\ \psi_{\text{int}}(r,\theta) = -r\sin\theta \dfrac{G}{c^2} \\ \qquad \times \left(\displaystyle\int_V \frac{j_\varphi(r',\theta')}{|\boldsymbol{r}-\boldsymbol{r}'|} dV' + \oint_S \frac{K_\varphi(r',\theta')}{|\boldsymbol{r}-\boldsymbol{r}'|} dS'\right) \end{cases} \tag{3.10}$$

As shown in the Appendix A, in spherical coordinates the scalar potential and the flux function are given in the external region ($r \to \infty$) in terms of standard multipole expansions

$$\begin{cases} \phi_{\text{ext}}(r,\theta) = -\dfrac{GM}{r}\left(1 + \displaystyle\sum_{k=1}^{n} Q_{2k}\left(\frac{r_0}{r}\right)^{2k} P_{2k}(\cos\theta)\right) \\ \psi_{\text{ext}}(r,\theta) = -\psi_0\left(1 + \displaystyle\sum_{k=1}^{n} M_{2k}\left(\frac{r_0}{r}\right)^{2k-1} C_{2k}^{(-1/2)}(\cos\theta)\right) \end{cases} \tag{3.11}$$

where $P_{2k}(\cos\theta)$ and $C_{2k}^{(-1/2)}(\cos\theta)$ denote Legendre and Gegenbauer polynomials, respectively. In the above expansions the scalar potential is assumed to vanish at infinity, while the flux function remains constant. If the flux function is also assumed to vanish at infinity the problem reduces to its Newtonian form. The external GE field is

$$\begin{aligned} \boldsymbol{E}_{\text{ext}}(r,\theta) &= -\nabla\phi_{\text{ext}}(r,\theta) \\ &= -\frac{\partial\phi_{\text{ext}}(r,\theta)}{\partial r}\widehat{\boldsymbol{r}} - \frac{1}{r}\frac{\partial\phi_{\text{ext}}(r,\theta)}{\partial\theta}\widehat{\boldsymbol{\theta}}, \end{aligned} \tag{3.12}$$

where

$$\begin{cases} \dfrac{\partial\phi_{\text{ext}}(r,\theta)}{\partial r} \\ \quad = \dfrac{GM}{r^2}\left(1 + \displaystyle\sum_{k=1}^{n}(2k+1)\,Q_{2k}\left(\frac{r_0}{r}\right)^{2k} P_{2k}(\cos\theta)\right) \\ \dfrac{\partial\phi_{\text{ext}}(r,\theta)}{\partial\theta} = \dfrac{GM}{r}\displaystyle\sum_{k=1}^{n}(2k+1)\,Q_{2k}\left(\frac{r_0}{r}\right)^{2k} \\ \quad \times\left(\dfrac{\cos\theta P_{2k}(\cos\theta) - P_{2k+1}(\cos\theta)}{\sin\theta}\right) \end{cases} \tag{3.13}$$

Likewise, the external GM field is

$$\begin{aligned} \boldsymbol{B}_{\text{ext}}(r,\theta) &= \nabla \times \boldsymbol{A}_{\text{ext}}(r,\theta) \\ &= \frac{1}{r^2\sin\theta}\left(\frac{\partial\psi_{\text{ext}}(r,\theta)}{\partial\theta}\widehat{\boldsymbol{r}} - r\frac{\partial\psi_{\text{ext}}(r,\theta)}{\partial r}\widehat{\boldsymbol{\theta}}\right), \end{aligned} \tag{3.14}$$

where

$$\begin{cases} \dfrac{\partial \psi_{\text{ext}}(r,\theta)}{\partial r} = \dfrac{\psi_0}{r_0}\displaystyle\sum_{k=1}^{n}(2k-1)\,M_{2k}\left(\dfrac{r_0}{r}\right)^{2k} C_{2k}^{(-1/2)}(\cos\theta) \\ \dfrac{\partial \psi_{\text{ext}}(r,\theta)}{\partial \theta} = -\psi_0\displaystyle\sum_{k=1}^{n} M_{2k}\left(\dfrac{r_0}{r}\right)^{2k-1}\sin\theta\, P_{2k-1}(\cos\theta) \end{cases} \tag{3.15}$$

Let $f(r,\theta) = f_0$ represent a surface of constant mass density. The normal to the surfaces $f(r,\theta)$ is given by

$$\widehat{\boldsymbol{n}} = \frac{\nabla f(r,\theta)}{\sqrt{\nabla f(r,\theta)\cdot\nabla f(r,\theta)}}, \tag{3.16}$$

so that the equivalent surface mass density $\sigma(r,\theta)$ and the equivalent surface mass current density $K_\varphi(r,\theta)$ can be evaluated just outside the fluid-vacuum interface $f(r,\theta) = 0$

$$\begin{cases} \sigma(r,\theta) = -\dfrac{\widehat{\boldsymbol{n}}\cdot\boldsymbol{E}_{\text{ext}}(r,\theta)}{4\pi G} = \dfrac{M}{4\pi r^2\sqrt{(r\partial f(r,\theta)/\partial r)^2 + (\partial f(r,\theta)/\partial\theta)^2}}\left\{ r\dfrac{\partial f(r,\theta)}{\partial r}\right. \\ \left. +\displaystyle\sum_{k=1}^{n}(2k+1)\,Q_{2k}\left(\dfrac{r_0}{r}\right)^{2k}\left[P_{2k}(\cos\theta)\,r\dfrac{\partial f(r,\theta)}{\partial r} + \left(\dfrac{\cos\theta P_{2k}(\cos\theta) - P_{2k+1}(\cos\theta)}{\sin\theta}\right)\dfrac{\partial f(r,\theta)}{\partial\theta}\right]\right\} \\ K_\varphi(r,\theta) = -\dfrac{c^2\,\widehat{\boldsymbol{n}}\times\boldsymbol{B}_{\text{ext}}(r,\theta)|_\varphi}{4\pi G} = \dfrac{r_0 I_0}{4\pi r^2\sin\theta\sqrt{(r\partial f(r,\theta)/\partial r)^2 + (\partial f(r,\theta)/\partial\theta)^2}} \\ \times\displaystyle\sum_{k=1}^{n} M_{2k}\left(\dfrac{r_0}{r}\right)^{2k-1}\left[(2k-1)\,C_{2k}^{(-1/2)}(\cos\theta)\,r\dfrac{\partial f(r,\theta)}{\partial r} - \sin\theta\,P_{2k-1}(\cos\theta)\dfrac{\partial f(r,\theta)}{\partial\theta}\right] \end{cases} \tag{3.17}$$

where $I_0 = c^2\psi_0/(Gr_0)$ is the total mass current defined in the Appendix A. The total mass M, the total mass current I_0, and the multipole coefficients Q_{2k} and M_{2k} can be determined in terms of the internal mass density $\rho(r,\theta)$ and the internal current density $j_\varphi(r,\theta)$ by solving Eqs. (A7) and (A10) of the Appendix A, just outside the fluid-vacuum interface. These equations are an application of the virtual casing principle and are here repeated for convenience:

$$\begin{cases} \displaystyle\int_V \frac{\rho(r',\theta')}{|\boldsymbol{r}(\theta)-\boldsymbol{r}'|}dV' \\ \quad = \dfrac{2M}{r(\theta)}\left(1+\displaystyle\sum_{k=1}^{n} Q_{2k}\left(\dfrac{r_0}{r(\theta)}\right)^{2k} P_{2k}(\cos\theta)\right) \\ \displaystyle\int_V \frac{j_\varphi(r',\theta')}{|\boldsymbol{r}(\theta)-\boldsymbol{r}'|}dV' = \dfrac{2r_0 I_0}{r(\theta)\sin\theta} \\ \quad\times\left(1+\displaystyle\sum_{k=1}^{n} M_{2k}\left(\dfrac{r_0}{r(\theta)}\right)^{2k-1} C_{2k}^{(-1/2)}(\cos\theta)\right) \end{cases} \tag{3.18}$$

Here, $\boldsymbol{r}(\theta)$ represents the fluid-vacuum interface obtained by a solution of $f(r,\theta) = 0$. Accordingly, the equivalent surface mass and surface mass current densities given by Eqs. (3.17) can be inserted in Eqs. (3.10) in order to determine the homogeneous part of the internal field distribution in terms of $\rho(r,\theta)$ and $j_\varphi(r,\theta)$. The integrals in Eqs. (3.10), as well as the integrals in Eqs. (3.18) can be expressed in terms of complete elliptic integrals using the explicit forms presented in Eq. (B2) of Appendix B. Finally, $\rho(r,\theta)$ and $j_\varphi(r,\theta)$ are connected in the internal region by the force balance Eq. (2.15) written in the form

$$\begin{aligned} &\rho(r,\theta)\,r\sin\theta\,(\nabla\times\widehat{\boldsymbol{\varphi}})\cdot\nabla\phi_{\text{int}}(r,\theta) \\ &\quad = j_\varphi(r,\theta)\,(\nabla\times\widehat{\boldsymbol{\varphi}})\cdot\nabla\psi_{\text{int}}(r,\theta), \end{aligned} \tag{3.19}$$

which is equivalent to Eq. (2.18) for the fluid velocity:

$$\begin{aligned} &r\sin\theta\left(r\frac{\partial\phi_{\text{int}}(r,\theta)}{\partial r} - \tan\theta\frac{\partial\phi_{\text{int}}(r,\theta)}{\partial\theta}\right) \\ &\quad = u_\varphi(r,\theta)\left(r\frac{\partial\psi_{\text{int}}(r,\theta)}{\partial r} - \tan\theta\frac{\partial\psi_{\text{int}}(r,\theta)}{\partial\theta}\right). \end{aligned} \tag{3.20}$$

The argument advanced at the end of Sect. 2 becomes clear with Eq. (3.19). The mass density $\rho(r,\theta)$ and the mass current density $j_\varphi(r,\theta)$ are related to the particular field solutions through the laws of Gauss and Ampère, while the oblique field components in the force balance Eq. (3.19) are related to the full internal fields $\phi_{\text{int}}(r,\theta)$ and $\psi_{\text{int}}(r,\theta)$ given by Eqs. (3.10). The oblique internal field components in Eq. (3.19) can be written in terms of complete elliptic integrals using Eqs. (B10) and (B12) of Appendix B.

The nonlinear system of integro-differential equations formulated in this section describes the equilibrium of a gravitationally contained rotating fluid dust with vanishing gravitational potential at infinity. A solution will be attempted in Sect. 5, but first some simplifications are introduced in the formulation regarding the hydro-gravitomagnetic Cauchy invariant and the conservation of energy.

4 Hydro-gravitomagnetic Cauchy invariance and conservation of energy

The circulation of the fluid velocity $\boldsymbol{u}$ is the line integral $\Gamma_f = \oint_\ell \boldsymbol{u}\cdot d\boldsymbol{\ell}$ around the closed curve ℓ. According to

Stokes' theorem, the circulation around a spheroidal circle of latitude ℓ corresponds to the poloidal flux of vorticity $\boldsymbol{\omega} = \boldsymbol{\nabla} \times \boldsymbol{u}$ passing trough the open latitudinal plane S

$$\int_S \boldsymbol{\omega} \cdot d\boldsymbol{S} = \iint_S (\boldsymbol{\nabla} \times \boldsymbol{u}) \cdot d\boldsymbol{S} = \oint_\ell \boldsymbol{u} \cdot d\boldsymbol{\ell} = 2\pi u_\varphi (r, \theta)\, r \sin\theta. \tag{4.1}$$

Similarly, the gravitomagnetic circulation $\Gamma_m = \oint_\ell \boldsymbol{A} \cdot d\boldsymbol{\ell}$ around the same curve ℓ corresponds to the poloidal flux of the gravitomagnetic field $\boldsymbol{B}$ passing trough S

$$\iint_S \boldsymbol{B} \cdot d\boldsymbol{S} = \iint_S (\boldsymbol{\nabla} \times \boldsymbol{A}) \cdot d\boldsymbol{S} = \oint_\ell \boldsymbol{A} \cdot d\boldsymbol{\ell} = 2\pi A_\varphi (r, \theta)\, r \sin\theta = 2\pi \psi (r, \theta). \tag{4.2}$$

The total canonical circulation in an axisymmetric equilibrium is

$$\Gamma = \oint_\ell (\boldsymbol{u} + \boldsymbol{A}) \cdot d\boldsymbol{\ell} = 2\pi \left[r \sin\theta u_\varphi (r, \theta) + \psi (r, \theta) \right]. \tag{4.3}$$

Now, the canonical vorticity $\boldsymbol{\Omega}$ of a fluid element is defined by the curl of the canonical momentum $\boldsymbol{P} = m(\boldsymbol{u} + \boldsymbol{A})$

$$\boldsymbol{\Omega} = \boldsymbol{\nabla} \times \boldsymbol{P} = m \boldsymbol{\nabla} \times (\boldsymbol{u} + \boldsymbol{A}) = m (\boldsymbol{\omega} + \boldsymbol{B}). \tag{4.4}$$

The present formulation is restricted to the weak relativistic approximation $\boldsymbol{u} \cdot \boldsymbol{u} \ll c^2$ due to the neglect of relativistic corrections in the fluid inertia. The ratio $\boldsymbol{\Omega}/\rho$ forms a Cauchy invariant $d(\boldsymbol{\Omega}/\rho)/dt = 0$ [24] so that, in steady state,

$$\boldsymbol{\nabla} \times (\boldsymbol{u} + \boldsymbol{A}) = \boldsymbol{C} \rho, \tag{4.5}$$

where $\boldsymbol{C}$ is a constant vector. Since the gradient of ρ does not vanish in general (compressible fluid dust), one must take $\boldsymbol{C} = 0$. It follows that the total canonical circulation Γ is null and

$$\frac{P_\varphi (r, \theta)}{m} = u_\varphi (r, \theta) + \frac{\psi (r, \theta)}{r \sin\theta} = 0 \tag{4.6}$$

inside the fluid. For an irrotational vortex $u_\varphi(r, \theta) = \mp\Gamma_0/(2\pi r \sin\theta)$, $\psi(r, \theta) = \pm\Gamma_0/(2\pi)$ (the flux is constant) and $\nabla \times u_\varphi (r, \theta) = 0$. For a rigid rotation $u_\varphi (r, \theta) = \mp\omega_0 r \sin\theta$, $\psi (r, \theta) = \pm\omega_0 r^2 \sin^2\theta$ (the flux is proportional to the equatorial area) and $\nabla \times u_\varphi (r, \theta) = \mp 2\omega_0 \sin\theta \widehat{\boldsymbol{\varphi}}$, where $\omega_0 = \Gamma_0/(2\pi r_0^2)$. The Cauchy invariance implies that everywhere inside the fluid

$$\psi_{\text{int}} (r, \theta) = -r \sin\theta u_\varphi (r, \theta). \tag{4.7}$$

Introducing the replacement $\psi_{\text{int}} (r, \theta) = -r \sin\theta u_\varphi (r, \theta)$, the force balance Eq. (3.20) becomes

$$\left(r \frac{\partial}{\partial r} - \tan\theta \frac{\partial}{\partial \theta} \right) \left(\frac{u_\varphi^2 (r, \theta)}{2} + \phi_{\text{int}} (r, \theta) \right) = 0, \tag{4.8}$$

which characteristic equation is

$$\frac{dr}{r} = -\frac{d\theta}{\tan\theta} \tag{4.9}$$

giving the characteristics

$$\frac{r}{r_0} \sin\theta = \text{constant}. \tag{4.10}$$

The general solution of Eq. (4.8) is

$$\frac{u_\varphi^2 (r, \theta)}{2} + \phi_{\text{int}} (r, \theta) = F \left(\frac{r}{r_0} \sin\theta \right), \tag{4.11}$$

where $F(r \sin\theta/r_0)$ is an arbitrary function (principal integral). The solution of the Cauchy problem (initial value problem) satisfying the boundary condition at the fluid-vacuum interface $r = r(\theta)$ gives the conservation of energy equation

$$\frac{u_\varphi^2 (r, \theta)}{2} + \phi_{\text{int}} (r, \theta) = \frac{u_\varphi^2 [r(\theta), \theta]}{2} + \phi_{\text{int}} [r(\theta), \theta]. \tag{4.12}$$

This equation is true for the irrotational vortex and rigid rotor cases. The gravitomagnetic field does not work directly (nevertheless, in non-stationary conditions the gravitoelectromotive force $-\partial \boldsymbol{A}/\partial t$ can do work on a test particle). In stationary conditions $u_\varphi (r, \theta)$ and $\psi_{\text{int}} (r, \theta)$ are linked to the scalar potential by the formulas

$$\begin{cases} u_\varphi (r, \theta) \\ \quad = \mp\sqrt{u_\varphi^2 [r(\theta), \theta] + 2 [\phi_{\text{int}} [r(\theta), \theta] - \phi_{\text{int}} (r, \theta)]} \\ \psi_{\text{int}} (r, \theta) \\ \quad = \pm r \sin\theta \sqrt{u_\varphi^2 [r(\theta), \theta] + 2 [\phi_{\text{int}} [r(\theta), \theta] - \phi_{\text{int}} (r, \theta)]} \end{cases} \tag{4.13}$$

These equations implicitly define the flow velocity and the gravitomagnetic flux in the internal region as functions of the gravitational potential (the gravitoelectric GE field) and the respective boundary conditions.

As a final comment, note that a further invariant can be implemented in general. The specific helicity associated with the canonical momentum $\boldsymbol{P}$ and the canonical vorticity $\boldsymbol{\Omega}$ is

$$\lambda = \boldsymbol{P} \cdot \boldsymbol{\Omega}. \tag{4.14}$$

Using the Reynolds transport theorem, the time variation of the total helicity $\Lambda = \int_V (\boldsymbol{P} \cdot \boldsymbol{\Omega})\, dV$ is given by

$$\frac{d\Lambda}{dt} = \frac{\partial}{\partial t} \int_V (\boldsymbol{P} \cdot \boldsymbol{\Omega})\, dV + \oint_S (\boldsymbol{P} \cdot \boldsymbol{\Omega})\, \boldsymbol{u} \cdot d\boldsymbol{S}, \tag{4.15}$$

so that in stationary conditions ($\partial/\partial t \equiv 0$) the total helicity Λ is invariant if the fluid velocity $\boldsymbol{u}$ is tangent to the surface $\boldsymbol{S}$. This is a generalization of Woltjer's theorem [45] which is true in the present problem since $u_\varphi \widehat{\boldsymbol{\varphi}}$ is tangent to $\boldsymbol{S}$. Due to axisymmetry, the specific helicity λ vanishes everywhere in the present case. Nevertheless, the invariance of Λ provides a further constraint in the case of spiral galaxies, for example.

5 Rotating oblate spheroids

The solution of the nonlinear system of integro-differential equations described in Sects. 3 and 4 leads to a consistent equilibrium of the gravitationally contained rotating fluid. The fluid-vacuum interface described by the function $f(r,\theta)=0$ is part of the solution, defining in general two classes of problems similar to the tokamak equilibrium problem [46,47]. In the fixed-boundary case the internal and external field distributions are determined in consistency with a given $f(r,\theta)=0$. In the free-boundary case the fluid-vacuum interface must be determined by an iterative procedure in order to satisfy the equilibrium equations as well as additional conditions and constraints such as given values of the total mass and total mass current (total angular momentum) contained in the system. The distinction between these two approaches is also pointed out by Drake and Turolla in obtaining interior solutions of the Kerr metric [48,49]. The expressions leading to a solution of the system in the gravitomagnetic context become cumbersome, so that a simple case will be considered in this section which illustrates the method of solution. This case corresponds to the gravitational equilibrium of a rotating oblate distribution of dust matter, which can be considered as a simple model for rotating globular or galaxy clusters. In fact, the boundary surface (virtual casing) examined by Drake and Turolla, for joining an unspecified interior structure to the exterior Kerr metric, corresponds exactly to the surface of an oblate spheroid [48]. One must mention that R.P. Kerr recently posted an article discussing the difficulties in constructing an interior solution to the Kerr metric [50].

The stationary state ($\partial/\partial t\equiv 0$) of a gravitationally contained rotating fluid with azimuthal symmetry ($\partial/\partial\varphi\equiv 0$) can be described assuming a given form for one of the four equilibrium variables, namely ρ, ϕ, ψ and u_φ in spherical polar coordinates (r,θ,φ). The simplest rotating gravitationally contained configuration corresponds to an oblate spheroid with constant mass density surfaces described by

$$f(r,\theta)=\frac{1}{r_0^2}\left[a^2(r)-\left(1-\frac{e^2}{2}\right)r^2-\left(\frac{e^2}{2}\right)r^2\cos 2\theta\right] \tag{5.1}$$

where $a(r)$ is the minor radius of the spheroidal surfaces and $0<e<1$ is the eccentricity. The eccentricity is kept constant so that the surfaces do not intersect. The mass density distribution is given by $\rho(r,\theta)=\rho_0 f(r,\theta)$, which vanishes at the boundary $0\leq\theta_b(r)\leq\pi$

$$\theta_b(r)=\frac{1}{2}\arccos\left(\frac{a^2(r)-\left(1-e^2/2\right)r^2}{\left(e^2/2\right)r^2}\right). \tag{5.2}$$

The mass density distribution has equatorial symmetry described by

$$\rho(r,\theta)=\rho_0(r)-\frac{\rho_0 e^2}{2}\left(\frac{r}{r_0}\right)^2\cos 2\theta. \tag{5.3}$$

This distribution vanishes at the fluid-vacuum interface defined by the first real root $r(\theta)$ of $\rho(r,\theta)=0$. The minor axis of the rotating spheroid is

$$a(r)=r_0\sqrt{\frac{\rho_0(r)}{\rho_0}+\left(1-\frac{e^2}{2}\right)\frac{r^2}{r_0^2}}, \tag{5.4}$$

and the major axis is $a(r)/\sqrt{1-e^2}$. This formulation corresponds to the class of fixed boundary equilibrium problems.

The scalar potential in the internal region is given by the sum of the particular and homogeneous solutions

$$\phi_{\text{int}}(r,\theta)=\phi_{\text{part}}(r,\theta)+\phi_{\text{hom}}(r,\theta). \tag{5.5}$$

The particular solution can be calculated in terms of the mass density $\rho(r,\theta)$ using the first term on the right-hand side of Eq. (B2) for $\phi_{\text{int}}(r,\theta)$ in the Appendix B

$$\phi_{\text{part}}(r,\theta)=-G\int_V\frac{\rho(r',\theta')}{|\boldsymbol{r}-\boldsymbol{r}'|}dV'=-G\int_0^{\pi}\int_0^{r(\theta')}\times\frac{4\rho(r',\theta')K\left[m(r,r';\theta,\theta')\right]r'^2\sin\theta'}{\sqrt{r^2+r'^2-2rr'\cos(\theta-\theta')}}dr'd\theta', \tag{5.6}$$

where $K(m)$ is the complete elliptic integral of the first kind as a function of the parameter $-1<m<1$

$$m(r,r';\theta,\theta')=-\frac{4rr'\sin\theta\sin\theta'}{\sqrt{r^2+r'^2-2rr'\cos(\theta-\theta')}}. \tag{5.7}$$

The particular solution is related to the multipole expansion at the fluid-vacuum interface $r=r(\theta)$ according to the first Eq. (3.18) for the scalar potential (the virtual casing principle)

$$\int_V\frac{\rho(r',\theta')}{|\boldsymbol{r}(\theta)-\boldsymbol{r}'|}dV'=\frac{2M}{r(\theta)}\left(1+\sum_{k=1}^{n}Q_{2k}\left(\frac{r_0}{r(\theta)}\right)^{2k}P_{2k}(\cos\theta)\right). \tag{5.8}$$

Note that an arbitrary function of the expression in the right-hand side has null tangential component of the gravitoelectric field. For a fixed boundary $r(\theta)$ the total mass M and the multipole coefficients Q_{2k} can be calculated in terms of the mass density distribution $\rho(r,\theta)$. Conversely, the multipole coefficients constitute the Dirichlet boundary condition for $\phi_{\text{part}}(r,\theta)$ at the interface $r(\theta)$. Taking the Fourier cosine series coefficients on both sides of this boundary condition leads to a set of linear equations linking the total mass M and the multipole coefficients Q_{2k} to the mass density profile:

$$\frac{2}{\pi}\left(\frac{2-\delta_{k,0}}{2}\right)\int_0^{\pi}\left(\int_V\frac{\rho(r',\theta')}{|\boldsymbol{r}(\theta)-\boldsymbol{r}'|}dV'\right)\cos 2k\theta\,d\theta$$

$$= \frac{2}{\pi}\left(\frac{2-\delta_{k,0}}{2}\right)\left(\frac{2M}{r_0}\right)\int_0^{\pi}\left(1 + \sum_{k=1}^{n} Q_{2k}\left(\frac{r_0}{r(\theta)}\right)^{2k} P_{2k}(\cos\theta)\right)\frac{r_0\cos 2k\theta}{r(\theta)}\,d\theta. \tag{5.9}$$

The integrals over θ in the above set of equations are calculated along the boundary $r(\theta)$ given by a solution of $\rho[r(\theta),\theta] = 0$. This set of $0 \leq k \leq n$ linear equations can be solved for M and Q_{2k} in terms of integrals of $\rho(r,\theta)$. Then, the first of equations (3.17) can be used to evaluate the equivalent surface mass density in terms of the multipole coefficients. For the mass density distribution given by Eq. (5.3) the surface mass distribution, related to the normal component of the gravitoelectric field, is given by (this specifies the Neumann boundary condition for the scalar potential)

$$\sigma(r,\theta) = \frac{M}{4\pi r^2\sqrt{\left(r\rho_0'(r) - e^2\rho_0 r^2\cos 2\theta/r_0^2\right)^2 + e^4\rho_0^2 r^4\sin^2 2\theta/r_0^4}}\left[r\rho_0'(r) - \frac{e^2\rho_0 r^2}{r_0^2}\cos 2\theta + \sum_{k=1}^{n}(2k+1)\,Q_{2k}\left(\frac{r_0}{r}\right)^{2k}\left(r\rho_0'(r)\,P_{2k}(\cos\theta) - \frac{e^2\rho_0 r^2}{r_0^2}\left(2\cos\theta\,P_{2k+1}(\cos\theta) - P_{2k}(\cos\theta)\right)\right)\right], \tag{5.10}$$

where $\rho_0'(r)$ denotes the derivative of the radial mass density distribution $\rho_0(r)$. Hence, using the second term on the right-hand side of Eq. (B2) for $\phi_{\text{int}}(r,\theta)$ the homogeneous term of the scalar potential is given by

$$\phi_{\text{hom}}(r,\theta) = -G\oint_S \frac{\sigma(r',\theta')}{|\boldsymbol{r}-\boldsymbol{r}'|}dS' = -G\int_0^{\pi}\frac{4\sigma\left[r(\theta'),\theta'\right]K\left[m\left(r,r(\theta');\theta,\theta'\right)\right]r(\theta')^2\sin\theta'}{\sqrt{r^2 + r(\theta')^2 - 2rr(\theta')\cos(\theta-\theta')}}d\theta', \tag{5.11}$$

which completes the calculation of the scalar potential in the internal region in terms of the mass density for fixed boundary conditions. In the external region the scalar potential is given in terms of the multipole expansion

$$\phi_{\text{ext}}(r,\theta) = -\frac{GM}{r}\left(1 + \sum_{k=1}^{n} Q_{2k}\left(\frac{r_0}{r}\right)^{2k} P_{2k}(\cos\theta)\right). \tag{5.12}$$

While these calculations give a solution of Gauss's law both in the internal and external regions for a given mass density distribution, a consistent equilibrium solution requires a full solution of the force balance (3.19) and a determination of the fluid flow velocity implicitly given by Eq. (4.13). With this in mind, note that the flux function in the internal region is given by the sum of particular and homogeneous solutions

$$\psi_{\text{int}}(r,\theta) = \psi_{\text{part}}(r,\theta) + \psi_{\text{hom}}(r,\theta). \tag{5.13}$$

The particular solution is given in terms of the mass current density $j_\varphi(r,\theta)$ by the first term on the right-hand side of Eq. (B2) for $\psi_{\text{int}}(r,\theta)$

$$\psi_{\text{part}}(r,\theta) = -r\sin\theta\frac{G}{c^2}\int_V \frac{j_\varphi\left(r',\theta'\right)}{|\boldsymbol{r}-\boldsymbol{r}'|}dV' = -r\sin\theta\frac{G}{c^2}\int_0^{\pi}\int_0^{r(\theta')} \times\frac{4j_\varphi\left(r',\theta'\right)K\left[m\left(r,r';\theta,\theta'\right)\right]r'^2\sin\theta'}{\sqrt{r^2+r'^2-2rr'\cos(\theta-\theta')}}dr'd\theta'. \tag{5.14}$$

The particular solution is also related to the multipole expansion just outside the fluid-vacuum interface of a rotating oblate spheroid (Dirichlet boundary condition for the particular flux function)

$$\int_V \frac{j_\varphi\left(r',\theta'\right)}{|\boldsymbol{r}(\theta)-\boldsymbol{r}'|}dV' = \frac{2r_0 I_0}{r(\theta)\sin\theta}\left(1 + \sum_{k=1}^{n} M_{2k}\left(\frac{r_0}{r(\theta)}\right)^{2k-1} C_{2k}^{(-1/2)}(\cos\theta)\right). \tag{5.15}$$

The Fourier cosine coefficients of this equation give a set of linear equations for the total current I_0 and the multipole coefficients M_{2k} in terms of integrals over $j_\varphi(r,\theta)$

$$\frac{2}{\pi}\left(\frac{2-\delta_{k,0}}{2}\right)\int_0^{\pi}\left(\int_V \frac{j_\varphi\left(r',\theta'\right)}{|\boldsymbol{r}(\theta)-\boldsymbol{r}'|}dV'\right)\cos(2k\theta)\,d\theta = \frac{2}{\pi}\left(\frac{2-\delta_{k,0}}{2}\right)2I_0\int_0^{\pi} \times\left(1 + \sum_{k=1}^{n} M_{2k}\left(\frac{r_0}{r(\theta)}\right)^{2k-1} C_{2k}^{(-1/2)}(\cos\theta)\right)\frac{r_0\cos(2k\theta)}{r(\theta)\sin\theta}\,d\theta. \tag{5.16}$$

Then, the equivalent surface mass current density, related to the tangential component of the gravitomagnetic field, is given by (this specifies the Neumann boundary condition for the flux function)

$$K_\varphi(r,\theta) = \frac{I_0\sin\theta}{4\pi r\sqrt{\left(r\rho_0'(r) - e^2\rho_0 r^2\cos 2\theta/r_0^2\right)^2 + e^4\rho_0^2 r^4\sin^2 2\theta/r_0^4}} \times\sum_{k=1}^{n} M_{2k}\left(\frac{r_0}{r}\right)^{2k}\left[r\rho_0'(r)\frac{(2k-1)\,C_{2k}^{(-1/2)}(\cos\theta)}{\sin^2\theta} - \frac{e^2\rho_0 r^2}{r_0^2}\left(\frac{(2k-1)\cos 2\theta\,C_{2k}^{(-1/2)}(\cos\theta)}{\sin^2\theta} + 2\cos\theta\,P_{2k-1}(\cos\theta)\right)\right],$$

(5.17)

so that, using the second term on the right-hand side of Eq. (B2) for $\psi_{\rm int}(r,\theta)$ the homogeneous part of the flux function in the internal region is given by

$$\begin{aligned}\psi_{\rm hom}(r,\theta) &= -r\sin\theta\frac{G}{c^2}\oint_S\frac{K_\varphi\left(r',\theta'\right)}{|\boldsymbol{r}-\boldsymbol{r}'|}dS'\\ &= -r\sin\theta\frac{G}{c^2}\int_0^\pi \\ &\times\frac{4K_\varphi\left[r\left(\theta'\right),\theta'\right]K\left[m\left(r,r\left(\theta'\right);\theta,\theta'\right)\right]r\left(\theta'\right)^2\sin\theta'}{\sqrt{r^2+r\left(\theta'\right)^2-2rr\left(\theta'\right)\cos\left(\theta-\theta'\right)}}d\theta'.\end{aligned} \tag{5.18}$$

In the external region the flux function is given by the gravitomagnetic multipole expansion (3.11)

$$\begin{aligned}\psi_{\rm ext}(r,\theta) &= -\frac{Gr_0I_0}{c^2}\\ &\times\left(1+\sum_{k=1}^{n}M_{2k}\left(\frac{r_0}{r}\right)^{2k-1}C_{2k}^{(-1/2)}(\cos\theta)\right).\end{aligned} \tag{5.19}$$

Now, in terms of the fluid velocity $u_\varphi(r,\theta)$ the force balance condition (3.19) in a general position (r,θ) inside the rotating oblate spheroid is given by

$$\begin{aligned}&r\sin\theta\left(\nabla\times\widehat{\boldsymbol{\varphi}}\right)\cdot\nabla\phi_{\rm int}(r,\theta)\\ &= u_\varphi(r,\theta)\left(\nabla\times\widehat{\boldsymbol{\varphi}}\right)\cdot\nabla\psi_{\rm int}(r,\theta).\end{aligned} \tag{5.20}$$

Taking the gradient of Eq. (3.10) and using the relations

$$\begin{aligned}&r\sin\theta\left(\nabla\times\widehat{\boldsymbol{\varphi}}\right)\cdot\nabla\left(r\sin\theta\right)=0 \quad\text{and}\\ &r\sin\theta\left(\nabla\times\widehat{\boldsymbol{\varphi}}\right)\cdot\left(\boldsymbol{r}-\boldsymbol{r}'\right)=r\cos\theta-r'\cos\theta'\end{aligned} \tag{5.21}$$

the force balance can be written in terms of integral relations

$$\begin{aligned}&\int_V\frac{\rho\left(r',\theta'\right)\left(r\cos\theta-r'\cos\theta'\right)}{|\boldsymbol{r}-\boldsymbol{r}'|^3}dV'\\ &+\oint_S\frac{\sigma\left(r',\theta'\right)\left(r\cos\theta-r'\cos\theta'\right)}{|\boldsymbol{r}-\boldsymbol{r}'|^3}dS'\\ &=\frac{u_\varphi(r,\theta)}{c}\left(\int_V\frac{j_\varphi\left(r',\theta'\right)}{c}\frac{\left(r\cos\theta-r'\cos\theta'\right)}{|\boldsymbol{r}-\boldsymbol{r}'|^3}dV'\right.\\ &\left.+\oint_S\frac{K_\varphi\left(r',\theta'\right)}{c}\frac{\left(r\cos\theta-r'\cos\theta'\right)}{|\boldsymbol{r}-\boldsymbol{r}'|^3}dS'\right),\end{aligned} \tag{5.22}$$

and finally in the form of a two-dimensional integral equation for the fluid velocity $u_\varphi(r,\theta)$

$$\begin{aligned}&\int_V\left(1-\frac{u_\varphi(r,\theta)}{c}\frac{u_\varphi\left(r',\theta'\right)}{c}\right)\frac{\rho\left(r',\theta'\right)\left(r\cos\theta-r'\cos\theta'\right)}{|\boldsymbol{r}-\boldsymbol{r}'|^3}dV'\\ &=-\oint_S\left(\sigma\left(r',\theta'\right)-\frac{u_\varphi(r,\theta)}{c}\frac{K_\varphi\left(r',\theta'\right)}{c}\right)\frac{\left(r\cos\theta-r'\cos\theta'\right)}{|\boldsymbol{r}-\boldsymbol{r}'|^3}dS'.\end{aligned} \tag{5.23}$$

The above integral equation shows the nonlinear nature of gravitational equilibrium, involving local and nonlocal contributions. If the projection $\left(\nabla\times\widehat{\boldsymbol{\varphi}}\right)\cdot\left[\boldsymbol{r}(\theta)-\boldsymbol{r}'\right]$ vanishes at all points of the fluid-vacuum interface the boundary surface has spherical symmetry with eccentricity $e=0$.

Performing the integration over the angle φ in polar spherical coordinates

$$\begin{aligned}&\int_0^{2\pi}\frac{d\varphi}{|\boldsymbol{r}-\boldsymbol{r}'|^3}\\ &=\frac{4E(m)}{\sqrt{r^2+r'^2-2rr'\cos\left(\theta-\theta'\right)}\left(r^2+r'^2-2rr'\cos\left(\theta+\theta'\right)\right)},\end{aligned} \tag{5.24}$$

the force balance condition can be written in terms of the complete elliptic integral of the second kind $E(m)$ as expressed by Eq. (B13). In the limit $r\to r'$ the integral

$$\begin{aligned}&\int_0^{2\pi}\frac{\left(r\cos\theta-r'\cos\theta'\right)d\varphi}{|\boldsymbol{r}-\boldsymbol{r}'|^3}\underset{r\to r'}{\longrightarrow}\\ &\times\frac{2\left(\cos\theta-\cos\theta'\right)}{r'^2\sqrt{2-2\cos\left(\theta-\theta'\right)}\left[1-\cos\left(\theta+\theta'\right)\right]}\\ &E\left(\frac{2\sin\theta\sin\theta'}{1-\cos\left(\theta-\theta'\right)}\right)\end{aligned} \tag{5.25}$$

has a non-integrable singularity at $\theta\to\theta'$ detailed in the Appendix C. The integral over the mass density, in the left-hand side of Eq. (5.23), gives a finite value since $\rho(r,\theta)$ vanishes at the fluid-vacuum interface. On the other hand, the singular behavior indicates that the term between parenthesis in the surface integral in the right-hand side of Eq. (5.23) must also vanish at the edge $(\boldsymbol{r}\to\boldsymbol{r}')$, in order to give a finite value to the integral. This consideration defines the rotation velocity at the fluid-vacuum interface as the ratio between the equivalent surface densities

$$u_\varphi\left[r(\theta),\theta\right]=\frac{c^2\sigma\left[r(\theta),\theta\right]}{K_\varphi\left[r(\theta),\theta\right]}=\frac{\widehat{\boldsymbol{n}}\cdot\boldsymbol{E}_{\rm ext}\left[r(\theta),\theta\right]}{\widehat{\boldsymbol{n}}\times\boldsymbol{B}_{\rm ext}\left[r(\theta),\theta\right]|_\varphi}. \tag{5.26}$$

Hence, the fluid velocity at the boundary of the oblate spheroid becomes

$$\begin{aligned}u_\varphi\left[r(\theta),\theta\right] &= \left(\frac{2c^2M}{r_0I_0}\right)\frac{r(\theta)}{r_0\sin\theta}\\ &\times\left[r(\theta)\rho_0'[r(\theta)]\left(1+\sum_{k=1}^{n}(2k+1)\,Q_{2k}\left(\frac{r_0}{r(\theta)}\right)^{2k}P_{2k}(\cos\theta)\right)\right.\\ &-\frac{e^2\rho_0r(\theta)^2}{r_0^2}\left(\cos2\theta+\sum_{k=1}^{n}(2k+1)\,Q_{2k}\left(\frac{r_0}{r(\theta)}\right)^{2k}\right.\\ &\left.\left.\times\left[2\cos\theta P_{2k+1}(\cos\theta)-P_{2k}(\cos\theta)\right]\right)\right]\\ &\times\left\{\sum_{k=1}^{n}M_{2k}\left(\frac{r_0}{r(\theta)}\right)^{2(k-1)}\left[r(\theta)\,\rho_0'[r(\theta)]\right.\right.\end{aligned}$$

$$\times \frac{2\left(2k-1\right) C_{2k}^{(-1/2)}\left(\cos\theta\right)}{\sin^2\theta} - \frac{e^2\rho_0 r\left(\theta\right)^2}{r_0^2}$$
$$\times \left(\frac{2\left(2k-1\right)\cos 2\theta\, C_{2k}^{(-1/2)}(\cos\theta)}{\sin^2\theta} + 4\cos\theta\, P_{2k-1}(\cos\theta)\right)\Bigg]\Bigg\}^{-1}. \tag{5.27}$$

Now, the constant density surfaces $r\left(\theta\right)$ of an oblate spheroid have extreme points $r\left(0\right) = r\left(\pi\right)$ on the axis and $r\left(\pi/2\right)$ on the equatorial plane. Taking the limits $\theta \to 0$ and $\theta \to \pi/2$ in Eq. (5.27) gives

$$u_\varphi\left[r\left(\theta\right),\theta\right] \underset{\theta\to 0}{\longrightarrow} \left(\frac{2c^2M}{r_0 I_0}\right)\frac{r\left(0\right)}{r_0\sin\theta}\left(1+\sum_{k=1}^{n}\left(2k+1\right)Q_{2k}\left(\frac{r_0}{r\left(0\right)}\right)^{2k}\right)$$
$$\times\left(\frac{r\left(0\right)\rho_0'\left[r\left(0\right),0\right] - e^2\rho_0 r^2\left(0\right)/r_0^2}{\sum_{k=1}^{n} M_{2k}\left(\frac{r_0}{r\left(0\right)}\right)^{2(k-1)}\left(\left(2k-1\right)r\left(0\right)\rho_0'\left[r\left(0\right),0\right] - \frac{\left(3+2k\right)e^2\rho_0 r\left(0\right)^2}{r_0^2}\right)}\right), \tag{5.28}$$

and

$$u_\varphi\left[r\left(\theta\right),\theta\right] \underset{\theta\to\pi/2}{\longrightarrow} \left(\frac{2c^2M}{r_0 I_0}\right)\frac{r\left(\pi/2\right)}{r_0}$$
$$\times\left(\frac{1+\sum_{k=1}^{n}\left(2k+1\right)Q_{2k}\left(\frac{r_0}{r(\pi/2)}\right)^{2k}P_{2k}(0)}{\sum_{k=1}^{n} M_{2k}\left(\frac{r_0}{r(\pi/2)}\right)^{2(k-1)} 2(2k-1)C_{2k}^{(-1/2)}(0)}\right), \tag{5.29}$$

where $r\left(0\right) = r_0\sqrt{1-e^2}$ is the external minor radius and $r\left(\pi/2\right) = r_0$ is the major radius of the oblate spheroid (minimum radial distance completely enclosing the mass distribution). Since $u_\varphi\left[r\left(\theta\right),\theta\right]$ must vanish for $\theta \to 0$ (this assumption may be relaxed in retrospect)), and noting that $\rho_0'\left(r,\theta\right)$ is negative at the edge, the first limit (5.28) implies that

$$1+\sum_{k=1}^{n}\frac{\left(2k+1\right)Q_{2k}}{\left(1-e^2\right)^k} = 0 \tag{5.30}$$

and the second limit (5.29) gives

$$u_\varphi\left(r_0,\frac{\pi}{2}\right) = \left(\frac{2c^2M}{r_0 I_0}\right)\left(\frac{1+\sum_{k=1}^{n}\left(2k+1\right)Q_{2k}P_{2k}\left(0\right)}{\sum_{k=1}^{n} 2\left(2k-1\right)M_{2k}C_{2k}^{(-1/2)}\left(0\right)}\right), \tag{5.31}$$

where $P_{2k}\left(0\right)$ and $C_{2k}^{(-1/2)}\left(0\right)$ can be calculated in terms of the Gamma function

$$\begin{cases} P_{2k}\left(0\right) &= \dfrac{\sqrt{\pi}}{\Gamma\left(\frac{1}{2}-k\right)\Gamma\left(1+k\right)} \\ C_{2k}^{(-1/2)}\left(0\right) &= -\dfrac{2^{2k-1}\Gamma\left(-\frac{1}{2}+k\right)}{\Gamma\left(\frac{1}{2}-k\right)\Gamma\left(1+2k\right)} \end{cases} \tag{5.32}$$

Therefore, the force balance for rotating oblate spheroids puts a constraint on the mass density profile in accordance with the first limit (5.28), namely,

$$Q_2 = -\left(\frac{1-e^2}{3}\right)\left(1+\sum_{k=2}^{n}\frac{\left(2k+1\right)Q_{2k}}{\left(1-e^2\right)^k}\right), \tag{5.33}$$

and provides a link between the fluid velocity at the equatorial edge of the mass density distribution and the GE and GM multipole coefficients in accordance with the second limit (5.29) in the form of Eq. (5.31).

Besides the mass density profile (and the fixed boundary defined by $\rho\left(r,\theta\right) = 0$), the velocity at the fluid-vacuum interface depends on the total mass M, the sum over the GE multipole coefficients Q_{2k} (linked to the eccentricity e), and the product of the total current I_0 by a sum over the GM multipole coefficients M_{2k}, which product is related to the strength of the external gravitomagnetic field

$$\boldsymbol{B}_{\text{ext}}\left(r,\theta\right) = -\left(\frac{GI_0}{c^2 r_0}\right)\frac{r_0^3}{r^3\sin\theta}\sum_{k=1}^{n} M_{2k}\left(\frac{r_0}{r}\right)^{2(k-1)}$$
$$\times\left[\sin\theta\, P_{2k-1}\left(\cos\theta\right)\widehat{\boldsymbol{r}} + \left(2k-1\right)C_{2k}^{(-1/2)}\left(\cos\theta\right)\widehat{\boldsymbol{\theta}}\right]. \tag{5.34}$$

The expansion of the flux function in the external region

$$\psi_{\text{ext}}\left(r,\theta\right) = -\frac{Gr_0 I_0}{c^2}\left(1+\sum_{k=1}^{n} M_{2k}\right.$$
$$\left.\times\left(\frac{r_0}{r}\right)^{2k-1} C_{2k}^{(-1/2)}\left(\cos\theta\right)\right) \tag{5.35}$$

shows that a constant flux related to the total current I_0 extends to infinity, while $\boldsymbol{B}_{\text{ext}}\left(r,\theta\right)$ decays like a sum of GM multipoles starting with a dipole. Likewise, the scalar

potential in the external region is

$$\phi_{\text{ext}}(r,\theta) = -\frac{GM}{r}\left(1+\sum_{k=1}^{n} Q_{2k}\left(\frac{r_0}{r}\right)^{2k} P_{2k}(\cos\theta)\right), \tag{5.36}$$

so that

$$\begin{aligned}\boldsymbol{E}_{\text{ext}}(r,\theta) &= -\frac{GM}{r^2} \\ &\times\left[\left(1+\sum_{k=1}^{n}(2k+1)\,Q_{2k}\left(\frac{r_0}{r}\right)^{2k} P_{2k}(\cos\theta)\right)\right. \\ &\widehat{\boldsymbol{r}} - \sum_{k=1}^{n}(2k+1)\,Q_{2k}\left(\frac{r_0}{r}\right)^{2k} \\ &\left.\times\left(\frac{P_{2k+1}(\cos\theta)-\cos\theta\,P_{2k}(\cos\theta)}{\sin\theta}\right)\widehat{\boldsymbol{\theta}}\right]\end{aligned} \tag{5.37}$$

decays like the sum of a monopole and higher order GE multipole terms, starting with a quadrupole.

The fluid velocity at the edge is given by Eq. (5.31) so that the Cauchy invariance condition (4.7) gives

$$\psi_{\text{int}}\left(r_0,\frac{\pi}{2}\right) = -\left(\frac{2c^2M}{I_0}\right)\left(\frac{1+\sum_{k=1}^{n}(2k+1)\,Q_{2k}P_{2k}(0)}{\sum_{k=1}^{n}2(2k-1)\,M_{2k}C_{2k}^{(-1/2)}(0)}\right), \tag{5.38}$$

which must be equal to the limit of the external flux function

$$\psi_{\text{ext}}\left(r_0,\frac{\pi}{2}\right) = -\frac{Gr_0I_0}{c^2}\left(1+\sum_{k=1}^{n}M_{2k}C_{2k}^{(-1/2)}(0)\right). \tag{5.39}$$

This gives the value of each GM multipole coefficient in terms of the total mass M, the total current I_0, and a sum of the GE multipole coefficients

$$\begin{aligned}M_{2k} &= -\frac{1}{2nC_{2k}^{(-1/2)}(0)} \\ &\left[1+\sqrt{1+4\left(\frac{2c^4M}{Gr_0I_0^2}\right)\frac{1}{2n}\left(1+\sum_{k=1}^{n}(k+1)\,Q_{2k}P_{2k}(0)\right)}\right].\end{aligned} \tag{5.40}$$

The flow velocity at the equatorial edge of the rotating dust configuration becomes (at arbitrary angular positions along the fluid-vacuum interface the truncated multipole expansions lead to large oscillations)

$$\begin{aligned}\frac{u_\varphi(r_0,\pi/2)}{c} &= -\frac{\left(\frac{c^3}{GI_0}\right)\left(\frac{2GM}{r_0c^2}\right)\frac{1}{n}\left(1+\sum_{k=1}^{n}(2k+1)\,Q_{2k}P_{2k}(0)\right)}{1+\sqrt{1+2\left(\frac{c^3}{GI_0}\right)^2\left(\frac{2GM}{c^2r_0}\right)\frac{1}{n}\left(1+\sum_{k=1}^{n}(2k+1)\,Q_{2k}P_{2k}(0)\right)}}.\end{aligned} \tag{5.41}$$

The flow velocity has been written in terms of the dimensionless current parameter GI_0/c^3 and the normalized Schwarzschild radius $2GM/c^2r_0$. This expression gives the same limit if either $2GM/c^2r_0 \ll 1$ or $GI_0/c^3 \gg 1$. The normalized Schwarzschild radius is less than one for non-black-hole objects, but the dimensionless current parameter can have any real value. The velocity has a discontinuous behavior associated with the gravitomagnetic field direction (angular velocity direction) for non-vanishing mass. This discontinuity can be easily identified assuming that the dimensionless parameter $GI_0/c^3 \ll 1$, resulting in an outer edge velocity of the order of the velocity of light times the square root of the normalized Schwarzschild radius

$$\begin{aligned}\frac{u_\varphi(r_0,\pi/2)}{c} &\approx -\text{sign}(I_0) \\ &\sqrt{\left(\frac{2GM}{c^2r_0}\right)\frac{1}{2n}\left(1+\sum_{k=1}^{n}(2k+1)\,Q_{2k}P_{2k}(0)\right)} \\ &+\frac{GI_0}{2c^3},\ \left|\frac{GI_0}{c^3}\right| \ll 1.\end{aligned} \tag{5.42}$$

In this case the velocity is weakly dependent of the total current I_0 necessary for equilibrium. Note the braking action of the gravitomagnetic field (Lenz's law), which acts besides providing the skew force for poloidal equilibrium. This braking effect is also responsible for giving the correct value of the anomalous perihelion shift in planetary motion [25]. The discontinuity associated with the gravitomagnetic field direction is present in the complex Newman-Janis transformation used by Drake [48] (the rotation parameter a of the transformation) in generating a stationary axially symmetric interior solution from spherically symmetric ones. Obviously, it is not possible to match an exterior Kerr metric to a completely static Schwarzschild metric (with rotation parameter $a = 0$) without incurring in some sort of singularity in the mass density profile. The change of geometry can only occur with the emission (possibly disruptive) of gravitational waves. This geometrical characteristic also occurs in the apparent disappearance of the relativistic perihelion shift for a transition from an elliptical to a circular orbital motion [25]. The above approximation for the total current I_0 completely disregards the actual mass density distribution.

Before attempting a solution of the full equilibrium, the outer edge velocity and the angular momentum will be estimated in the next section by introducing a simple model for the mass distribution.

6 Velocity and angular momentum versus mass

The total current can be estimated first solving I_0 in terms of M from Eq. (5.41)

$$\frac{GI_0}{c^3} = -\frac{1}{\beta_\varphi}\left(\frac{2GM}{c^2 r_0}\right)\frac{1}{2n} \times\left(1+\sum_{k=1}^{n}(2k+1)\,Q_{2k}P_{2k}\,(0)\right)+\beta_\varphi, \tag{6.1}$$

if

$$0<\beta_\varphi^2<\left(\frac{2GM}{c^2 r_0}\right)\frac{1}{2n}\left(1+\sum_{k=1}^{n}(2k+1)\,Q_{2k}P_{2k}\,(0)\right), \tag{6.2}$$

where $\beta_\varphi = u_\varphi\,(r_0,\pi/2)/c$. This is an exact solution for the oblate spheroid. Now, it can be assumed that the mass M is distributed on a relativistic ring of radius r_0 rotating with the velocity u_φ, so that

$$I_0 \sim -\frac{M}{2\pi r_0}\frac{u_\varphi}{\sqrt{1-u_\varphi^2/c^2}} \Longrightarrow \frac{GI_0}{c^3}\sim -\frac{1}{4\pi}\left(\frac{2GM}{c^2 r_0}\right)\frac{\beta_\varphi}{\sqrt{1-\beta_\varphi^2}}. \tag{6.3}$$

Note that the mass of the ring has been corrected by the Lorentz factor $\gamma = 1/\sqrt{1-\beta_\varphi^2}$. This is not completely consistent with the calculations in the previous sections, where the relativistic correction in the fluid inertia was neglected. Nevertheless, the relativistic ring assumption partially reintroduces the relativistic effects in the high normalized Schwarzschild radius range $2GM/c^2 r_0 \lesssim 1$. With the above replacement for I_0, the velocity β_φ can be calculated solving the equation

$$\frac{1}{4\pi}\left(\frac{2GM}{c^2 r_0}\right)\frac{\beta_\varphi}{\sqrt{1-\beta_\varphi^2}} \approx \frac{1}{\beta_\varphi}\left(\frac{2GM}{c^2 r_0}\right)\frac{1}{2n}\left[\frac{3-e^2}{2} +\sum_{k=2}^{n}(2k+1)\,Q_{2k}\left(\frac{1}{2\left(1-e^2\right)^{k-1}}+P_{2k}\,(0)\right)\right]-\beta_\varphi, \tag{6.4}$$

where the mass density profile constraint (5.33) was used. This gives a cubic equation for β_φ^2 with coefficients depending on the normalized Schwarzschild radius $2GM/c^2 r_0$, the eccentricity e, and a sum of higher order GE multipole coefficients. The cubic equation is best solved by numerical methods. One may consider a further idealized condition where the external GE field is represented by the sum of monopole M and quadrupole $Q_2 = -\left(1-e^2\right)/3$ terms only, so that $n=1$ and all higher order terms $k\geq 2$ can be neglected. This situation is possible, but requires a mass density profile with a higher order spectral representation in place of the simple distribution (5.3). In any case, the mass ring approximation corresponds to such a complex representation. The implication of these approximations is a poor fitting of the boundary conditions at the fluid-vacuum interface of the oblate spheroid, but sufficient for velocity estimation using the simplified equation

$$\frac{1}{4\pi}\left(\frac{2GM}{c^2 r_0}\right)\frac{\beta_\varphi}{\sqrt{1-\beta_\varphi^2}} \approx \frac{1}{\beta_\varphi}\left(\frac{2GM}{c^2 r_0}\right)\left(\frac{3-e^2}{4}\right)-\beta_\varphi. \tag{6.5}$$

For small values of $2GM/c^2 r_0$ in the nonrelativistic limit this equation agrees with the force balance condition used by Oepik [51] to determine the distance to the Andromeda galaxy, eventually leading to the Tully–Fisher relation [52].

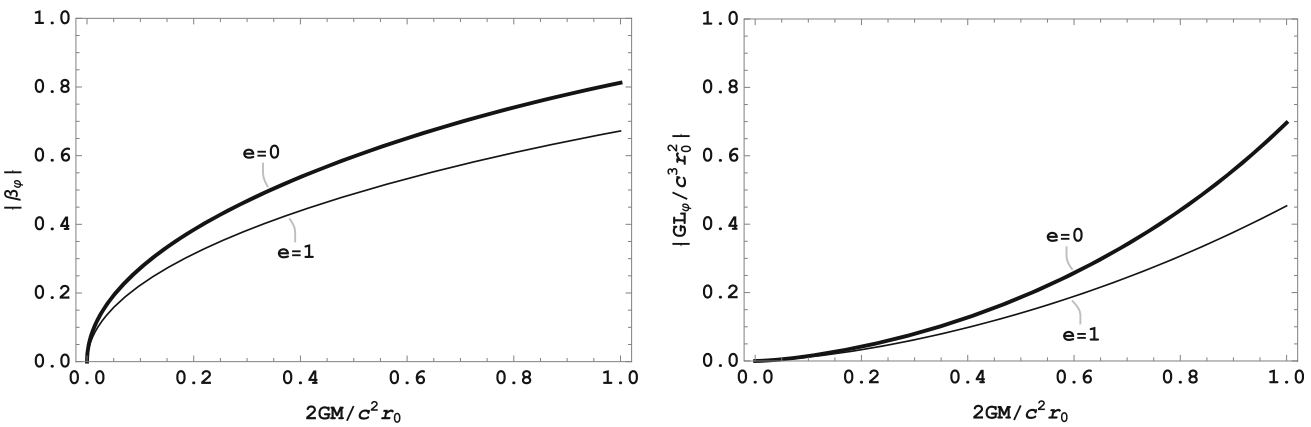

Fig. 1 Velocity (left-hand panel) and normalized angular momentum (right-hand panel) versus normalized Schwarzschild radius for a ring current. The curves correspond to the full range of values of the eccentricity e

The gravitomagnetic field at the outer equatorial edge is given by

$$\boldsymbol{B}_{\text{ext}}\left(r_0, \frac{\pi}{2}\right) = -\frac{c}{2r_0}\left(\frac{GI_0}{c^3}\right) \times \sum_{k=1}^{n} 2\,(2k-1)\,M_{2k} C_{2k}^{(-1/2)}\,(0)\,\widehat{\boldsymbol{\theta}}, \tag{6.6}$$

with M_{2k} replaced by Eq. (5.40). As demonstrated in Sect. 4, the canonical vorticity is null for compressible dust in stationary flow. The canonical vorticity is a Cauchy invariant, establishing an exchange between the fluid and field vorticities in the internal region. In the vacuum region the fluid vorticity vanishes, but not the field vorticity in general, which is sustained by the internal rotating fluid distribution (or vice-versa). If the model is extended to an observable universe this finding is in accordance with the very low limits of matter vorticity extracted from the cosmic microwave background (CMB) data [53]. Nevertheless, the fluid vorticity does not vanish in the internal region, and the total mechanical angular momentum for a mass M rotating on a circular loop of radius r_0 can be calculated multiplying the moment of inertia by the angular velocity. The normalized angular momentum of a relativistic current ring is given by

$$\frac{GL_\varphi}{c^3 r_0^2} = \frac{1}{2}\left(\frac{2GM}{c^2 r_0}\right)\frac{\beta_\varphi}{\sqrt{1-\beta_\varphi^2}}. \tag{6.7}$$

If the mass M is uniformly distributed on a disk, the moment of inertia decreases and the angular momentum value must be multiplied by a factor $1/2$. For a spherical shell the multiplying factor would be $2/3$. The correct factor depends on the integration of the flow velocity u_φ at the surface of the rotating dust configuration. In the present ring model the eccentricity $0 < e < 1$ is just part of this adjusting factor. Figure 1 shows the variation of β_φ and $GL_\varphi/c^3 r_0^2$ as functions of the normalized Schwarzschild radius $2GM/c^2 r_0$, and of the eccentricity e. The rotation velocity increases significantly even for small anisotropism. The velocity tends asymptotically towards the velocity of light for large values of $2GM/c^2 r_0$. Of course, strong relativistic effects cannot be ignored at the upper end. Figures 2 and 3 show the variation of the normalized angular momentum of a rotating mass ring versus mass, for the extreme values of e, and a few adjustments using the correlation proposed by Brosche for a wide variety of astronomical objects, from planet-satellite systems, double stars, rotating globular and galaxy clusters, up to superclusters [54]

$$\left|\frac{GL_\varphi}{c^3 r_0^2}\right| \simeq a\left(\frac{2GM}{c^2 r_0}\right)^b. \tag{6.8}$$

A re-examination of experimental results puts a value of b for the Brosche correlation in the range $1.5 < b < 2.0$, exactly as shown in Figs. 2 and 3, leading to the Trimble correlations [55]. These figures indicate that higher values of $b \lesssim 2.0$ give a good fit in the very high mass range, while small values of $b \gtrsim 1.5$ give a better fit in the low mass range. A two terms expansion of the angular momentum for $2GM/c^2 r_0 \ll 1$ is given by

$$\left|\frac{GL_\varphi}{c^3 r_0^2}\right| \approx \frac{1}{4}\sqrt{3\left(1-\frac{e^2}{3}\right)}\left(\frac{2GM}{c^2 r_0}\right)^{3/2} - \frac{1}{32\pi}\left[1-3\pi\left(1-\frac{e^2}{3}\right)\right]\sqrt{3\left(1-\frac{e^2}{3}\right)}\left(\frac{2GM}{c^2 r_0}\right)^{5/2} + \ldots \tag{6.9}$$

The leading term in this expansion gives

$$\ln\left|\frac{GL_\varphi}{c^3 r_0^2}\right| \approx \ln\left(\frac{1}{4}\sqrt{3\left(1-\frac{e^2}{3}\right)}\left(\frac{2G}{c^2 r_0}\right)^{3/2}\right) + \frac{3}{2}\ln M, \qquad \frac{2GM}{c^2 r_0} \ll 1, \tag{6.10}$$

which corresponds to the relation between angular momentum and mass for "terrestrial" objects [55]. The normalized angular momentum versus mass relation can be used to estimate the mass of large astrophysical objects from the measured size and edge rotation velocity. The angular momentum for a ring of distributed mass is calculated using Eq. (6.7), while the rotation velocity at the edge is given either by Eq. (6.4) or the simplified Eq. (6.5), which replaces the Tully–Fisher relation [52] for mass estimation. As pointed out previously, in the nonrelativistic limit and for small values of $2GM/c^2 r_0$ Eq. (6.5) reduces to

$$\beta^2 \approx \frac{3}{4}\left(1-\frac{e^2}{3}\right)\left(\frac{2GM}{c^2 r_0}\right). \tag{6.11}$$

The luminosity of galaxies is measured over a disk of radius r_0, encompassing a mass $M \propto r_0^2$ (an application of Abel transform). It follows that $\beta_{obs}^4 \propto M$, in accordance with the baryonic Tully–Fisher relation [56], and $L_{\varphi,\text{obs}} \propto M^{7/4}$. Note that the nonrelativistic relations $M = k u_\varphi^2 r_0/G$ and $L_\varphi = k' G^{1/2} r_0^{1/2} M^{3/2}$, with dimensionless constants k and k', can be obtained by simple dimensional analysis (Buckingham's π theorem). Then, application of the Abel transform indicates that the observed astrophysical values should follow the laws $u_\varphi \propto M^{1/4}$ and $L_\varphi \propto M^{7/4}$. Adding the speed of light to the dimensional analysis introduces the new dimensionless variable $\beta = u_\varphi/c$, showing that in the relativistic case the normalized Schwarzschild radius $2GM/c^2 r_0$ is an arbitrary function of β^2, which reduces to a proportionality relation in the nonrelativistic limit as illustrated in Fig. 1 (the proportionality factor depends on the moment of inertia).

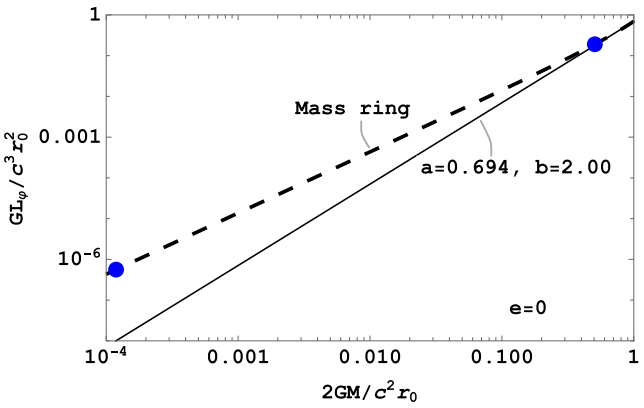

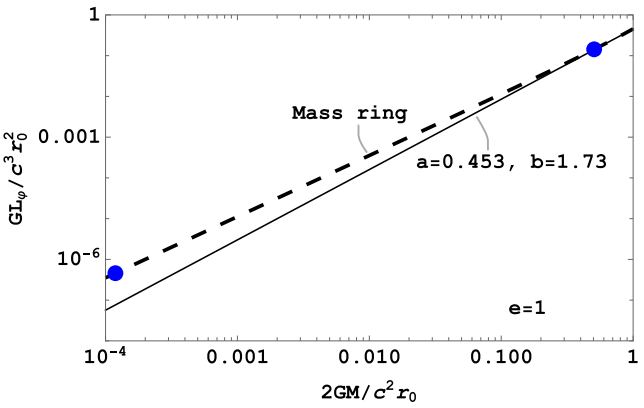

Fig. 2 Normalized angular momentum versus normalized Schwarzschild radius for a rotating mass ring. The left-hand panel shows the angular momentum versus mass variation for a rotating mass ring (dashed line) with $e = 0$. An adjustment in the very high range of mass values, using the well known Brosche model [54] is also displayed (thin line). The right-hand panel shows the value and the high mass range adjustment for $e = 1$. The lower-left point indicates the position of the Laniakea supercluster, with a radius $r_0 \simeq 2.5 \times 10^{24}$ m and total mass $M \simeq 2.0 \times 10^{47}$ kg [57]. The upper-right point corresponds to an observable universe with a radius $r_0 \simeq 4.4 \times 10^{26}$ m and total mass $M \simeq 1.5 \times 10^{53}$ kg

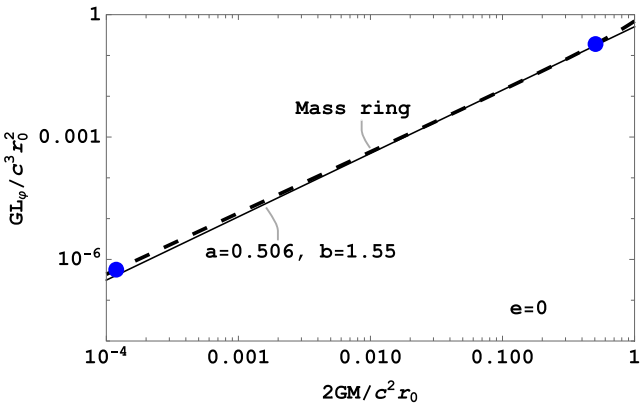

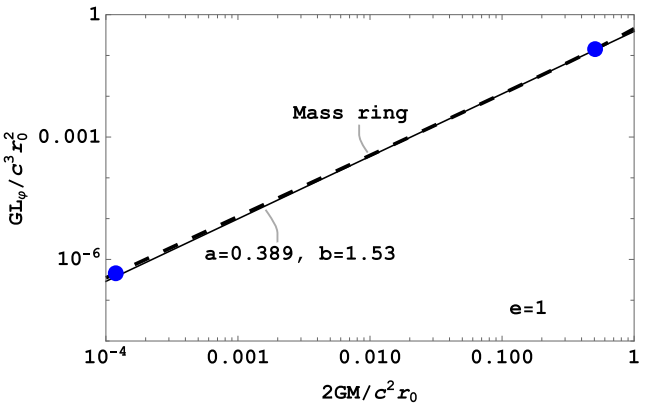

Fig. 3 Normalized angular momentum versus normalized Schwarzschild radius for a rotating mass ring. The left-hand panel shows the angular momentum versus mass variation for a rotating mass ring (dashed line) with $e = 0$. An adjustment strongly weighted towards the low range of mass values, is also displayed (thin line). The right-hand panel shows the value and the low mass range adjustment for $e = 1$. The lower-left point indicates the position of the Laniakea supercluster, with a radius $r_0 \simeq 2.5 \times 10^{24}$ m and total mass $M \simeq 2.0 \times 10^{47}$ kg. The upper-right point corresponds to an observable universe with a radius $r_0 \simeq 4.4 \times 10^{26}$ m and total mass $M \simeq 1.5 \times 10^{53}$ kg

Similar conclusions were reached by Srivastava et al using a stationary, axially-symmetric Weyl metric formulation [26]. Note that the simple approximations for a mass M distributed on a ring or a disk do not take into account the detailed mass density distribution $\rho\,(r, \theta)$, but show that the gravitoelectromagnetic approximation should be adequate to describe the dynamics of extended astrophysical objects, up to and possibly beyond superclusters. The dependence of an extended gravitational system on the detailed mass distribution is the subject of the next section.

7 Extended gravitational system—a large rotational vortex

Here, a monotonic Gaussian profile is implemented to describe the mass density distribution of an extended gravitational system in stationary rotation. As such, consider a rotating oblate spheroid with a minor radius described by the combined Gaussian profile

$$a(r) = r_0 \sqrt{1 - \frac{\exp\left(\frac{1}{2\alpha^2}\right) - \exp\left[\frac{1}{2\alpha^2}\left(1-\frac{r^2}{r_0^2}\right)\right]}{\exp\left(\frac{1}{2\alpha^2}\right) - 1} + (1-e^2)\frac{r^2}{r_0^2}}, \tag{7.1}$$

so that in accordance with Eq. (5.1) the mass density is given by

$$\rho\left(r,\theta\right)=\rho_0\left[\frac{a\left(r\right)^2}{r_0^2}-\left(1-\frac{e^2}{2}\right)\frac{r^2}{r_0^2}\right]-\frac{\rho_0 e^2}{2}\frac{r^2}{r_0^2}\cos 2\theta. \tag{7.2}$$

The Gaussian profile depends both on the eccentricity e and the parameter α. Figure 4 shows the normalized mass density along the equatorial plane for the particular values $e=0.715002$ and $\alpha=0.466450$. By construction the mass density drops to zero at the finite radius r_0 along the equatorial plane $\theta=\pi/2$ (r_0 is the minimum radial distance completely enclosing the mass distribution). The parameter α is numerically determined as a function of e so that $a\left(r_0\sqrt{1-e^2}\right)=r_0\sqrt{1-e^2}$, that is, so that $a\left(r\right)$ gives $\rho\left(r_0\sqrt{1-e^2},0\right)=0$ at the minor axis position $r_0\sqrt{1-e^2}$ on the axis $\theta=0$. Figure 4 shows also how the parameter α varies as a function of e for the assumed profile. In this way, the normalized mass density profile is defined by the eccentricity e only. For very large values of α the Gaussian profile is approximately given by

$$\rho(r,\theta)\underset{\alpha\gg 1}{\simeq}\rho_0\left\{1-\left[1+\frac{e^2}{2}+\frac{1}{4\alpha^2}\left(1-\frac{r^2}{r_0^2}\right)\right]\frac{r^2}{r_0^2}-\frac{e^2}{2}\frac{r^2}{r_0^2}\cos 2\theta\right\}, \tag{7.3}$$

and e must be small so that the density vanishes for $\theta=0$ and $r=r_0\sqrt{1-e^2}$:

$$e\underset{\alpha\gg 1}{\simeq}\frac{1}{\sqrt{4\alpha^2+1}}\;;\;\alpha\underset{e\ll 1}{\simeq}\frac{\sqrt{1-e^2}}{2e}. \tag{7.4}$$

For $\alpha\to\infty$ and $e\to 0$ the density reduces to a parabolic distribution inside a sphere of radius r_0 (with a discontinuous change in the curvature). Now, the eccentricity e is determined by the constraint (5.33) imposed by the force balance condition. The value of e must be determined by an iterative procedure together with a solution of Gauss's law for the gravitational scalar potential $\phi\left(r,\theta\right)$ that satisfies the boundary conditions, as detailed in the following.

As described in Sect. (5), the total mass M and the multipole coefficients Q_{2k} can be calculated taking the Fourier cosine coefficients of the Dirichlet boundary condition (5.8) for the particular solution $\phi_{\text{part}}\left(r,\theta\right)$. This is a direct application of the virtual casing principle. In the present section the particular solution is evaluated using the above Gaussian profile (7.1) for $\rho\left(r,\theta\right)$ with an initial guessed eccentricity e, forming a set of linear equations for M and Q_{2k}. Note that the particular solution integral spans the mass density profile up to the fluid-vacuum interface $r_b\left(\theta\right)$ defined by the first real root of $\rho\left(r,\theta\right)=0$. Then, a new value e' for the eccentricity is calculated using the constraint (5.33) on the mass density profile. An approximation of e can be successively improved by iteration using a regula falsi method. In the present case, the numerical procedure leads to the set of parameters presented in Table 1, truncated to ten multipoles ($n=10$). Figures 5 and 6 show the final result of the computation. The advantage of this solution method is that a simple analytical expression for $\rho\left(r,\theta\right)$ is obtained which satisfies Gauss's law and the force balance equation. For a given assumed shape the final solution is completely defined. Considering the value obtained for the normalized Schwarzschild radius, $r_S=2GM/(c^2r_0)=0.6457$, one verifies that the Gaussian profile (7.1) may represent the mass distribution of a hypothetical observable universe in stationary conditions

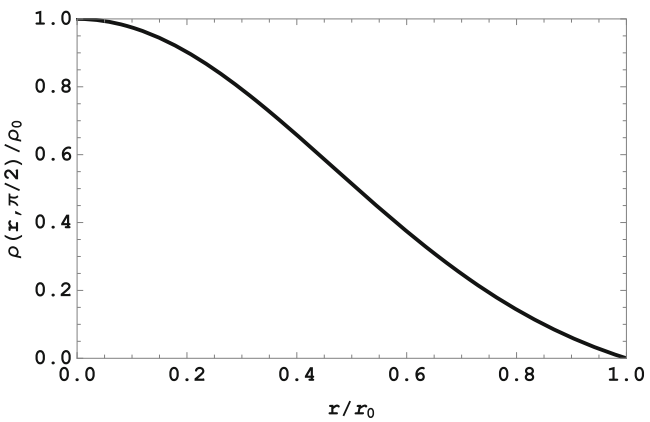

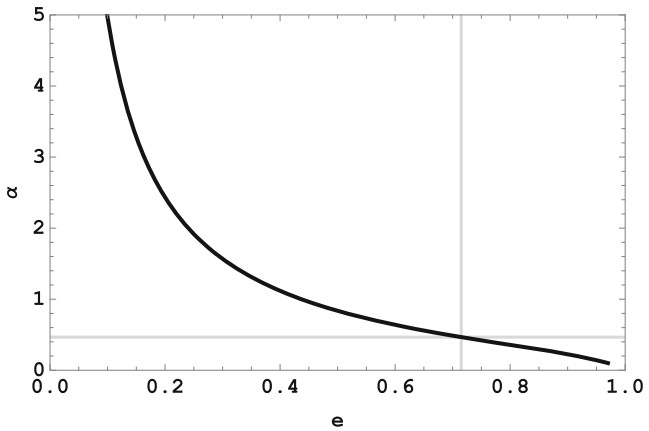

Fig. 4 Normalized mass density profile along the equatorial plane for a constrained Gaussian distribution (left-hand panel). Relation between the Gaussian profile parameter α and the eccentricity e (right-hand panel). This relation ensures that the mass density vanishes at the major and minor axes positions on the fluid-vacuum interface. The grid lines indicate the pair of values $e=0.715002$ and $\alpha=0.466450$ giving a consistent equilibrium with the assumed Gaussian shape

Table 1 Profile parameters and multipoles expansion of an extended gravitational system. The table gives the eccentricity e and the parameter α characterizing the Gaussian mass density distribution described in the text for and extended gravitational system. The table also gives the normalized mass $GM/(c^2 r_0)$ and the first ten multipoles Q_{2k} ($k = 1, 2...10$) of the truncated solution displayed in Figs. 5 and 6. The multipoles converge slowly to zero with alternating signs

e	α	$GM/(c^2 r_0)$	Q_2	Q_4	Q_6	Q_8
0.715002	0.466450	0.322828	0.0318408	− 0.0921019	0.0677537	− 0.0444411
Q_{10}	Q_{12}	Q_{14}	Q_{16}	Q_{18}	Q_{20}	
0.028471	− 0.0177264	0.0104307	− 0.00530854	0.00202209	− 0.000390967	

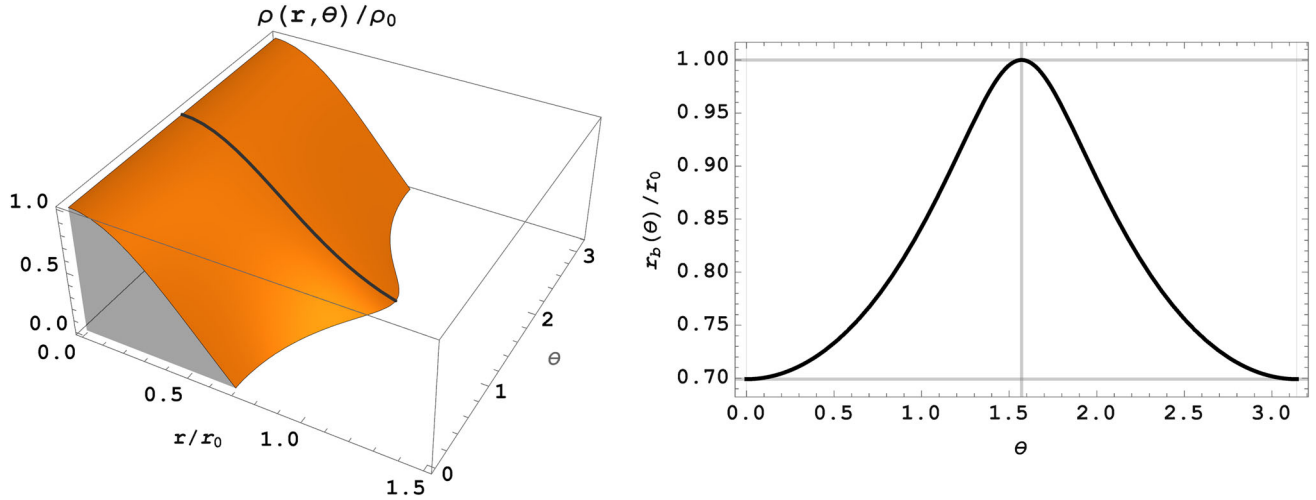

Fig. 5 Mass density of an extended gravitational system. The left-hand panel shows the normalized mass density distribution in spherical coordinates (r, θ). The right-hand panel shows the radial position $r_b\,(\theta)\,/r_0$ of the fluid-vacuum interface. The equatorial radius r_0 corresponds to the minimum radial distance completely enclosing the mass distribution. The minor radius of the containing oblate spheroid is $r_0\sqrt{1-e^2}$

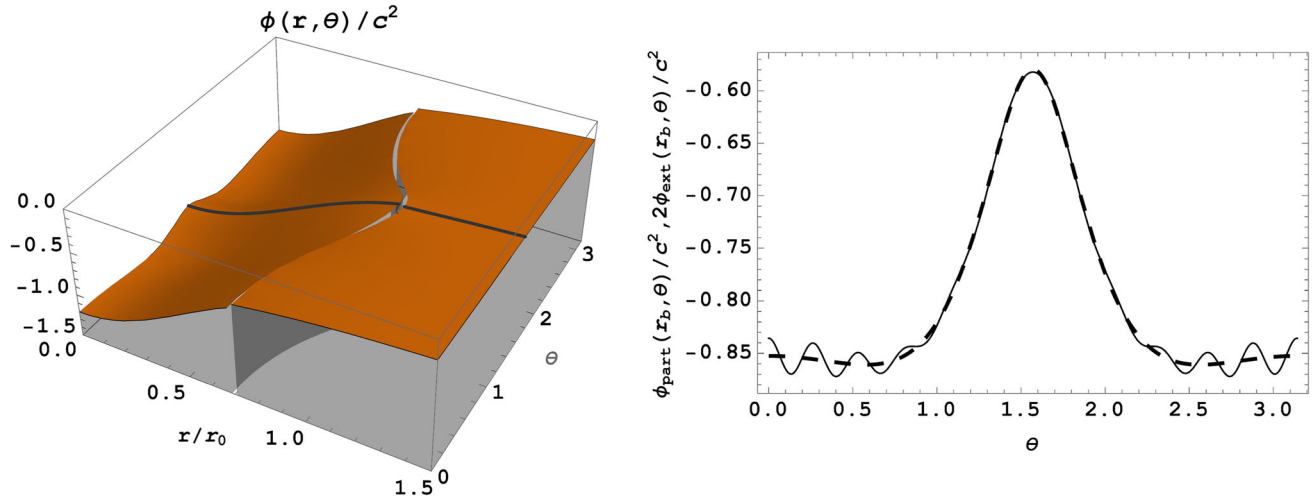

Fig. 6 Gravitational potential of an extended gravitational system. The left-hand panel shows the normalized scalar potential corresponding to the mass density of Fig. 5. The displayed exclusion indicates the fluid-vacuum interface, with the internal potential extending to the left and the external potential to the right of the interface (into the vacuum region). The right-hand panel shows the particular potential (dashed line) and twice the external potential (thin continuous line) along the fluid-vacuum interface (virtual casing). The external potential corresponds to the truncated multipoles expansion given in Table 1. Clearly, a large number of multipoles is needed to adjust the external potential near the interface (notably near the axis of rotation)

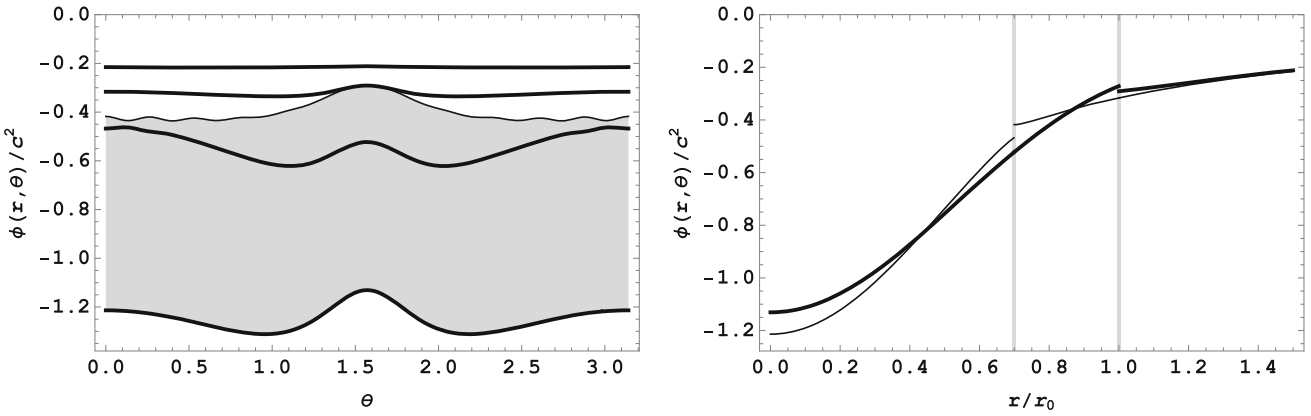

Fig. 7 The left-hand panel shows the scalar potential profiles along the poloidal angle θ for selected values of the radial distance r. The thick lines correspond, from bottom to top, to $r = 0$, $r = r_0\sqrt{1-e^2}$, $r = r_0$ and $r = 3r_0/2$. The shaded region corresponds to the internal region with the scalar potential given by $\phi_{\rm int}(r,\theta)$. In the external region the (negative) scalar potential $\phi_{\rm ext}(r,\theta)$ decays monotonically to zero. The thin line corresponds to the profile along the fluid-vacuum interface using the truncated expansion for $\phi_{\rm ext}(r,\theta)$ ($n = 10$). This profile shows the oscillations produced by the truncated multipole expansion. A larger number of multipole components reduces the amplitude of the oscillations at the expense of increasing their number. At the extreme points $\theta = 0$ and $\theta = \pi$ the thin line at the interface and the thick line for $r = r_0\sqrt{1-e^2}$ converge to the same value as $n \to \infty$, but differ for finite n. The right-hand panel shows the scalar potential radial profiles for $\theta = \pi/2$ (thick line) and $\theta = 0$ (thin line). The vertical lines indicate the small discontinuities associated with the oscillations in the truncated external potential

(cf. Figs. 2 and 3). Further improvements should be obtained by including relativistic corrections in the fluid inertia and proper mass density profiles. Note that the present configuration is not intended as a cosmological model, it just illustrates the applicability of the gravitomagnetic formulation in the description of very large gravitational systems.

The gravitational potential shown in Fig. 6 is calculated using Eqs. (5.6), (5.11) and (5.12). Figure 7 shows the poloidal and radial profiles of the scalar potential shown in Fig. 6. Both Figs. 6 and 7 indicate that a large number of multipole components are needed to properly represent the external scalar potential and satisfy the boundary condition at the fluid-vacuum interface. The present representations are limited to ten multipoles ($n = 10$).

One must keep in mind that the gravitational GE equilibrium has two free parameters, the size parameter r_0 and the reference density ρ_0. The values listed in Table 1 were calculated assuming $r_0 = 1$ and $\rho_0 = 1$ (with c=1 and G=1). Smaller values of ρ_0 correspond to proportionally smaller values of M and ϕ, without changing the geometrical values in Table 1. The values of ϕ in Figs. 6 and 7 change accordingly. The size r_0 of the system and the normalized Schwarzschild radius $2GM/c^2r_0$ define the consistent GE equilibrium for an assumed shape of the density distribution. For example, the ratio between the normalized Schwarzschild radii for the Laniakea supercluster and the observable universe shown in Figs. 2 and 3 is $\sim 2.3\times10^{-4}$, but both systems can in principle be described by the same Gaussian profile (7.1). Now, the gravitomagnetic GM equilibrium introduces a third free parameter in the form of the normalized total current GI_0/c^3 (total angular momentum). The flux function and the gravitomagnetic field are proportional to I_0, but the rotational velocity has a nonlinear dependence both on the total mass M and the total current I_0.

The flow velocity at the equatorial edge is calculated by the ratio (5.26) between the radial component of the GE field and the rotated poloidal component of the GM field. Using Eqs. (5.34), (5.37) and (5.40)

$$\begin{aligned}\frac{u_\varphi\,(r_0,\pi/2)}{c} &= \frac{\widehat{\boldsymbol{r}}\cdot\boldsymbol{E}_{\rm ext}\,(r_0,\pi/2)}{c\,\widehat{\boldsymbol{r}}\times\boldsymbol{B}_{\rm ext}\,(r_0,\pi/2)|_\varphi}\\ &= \left(\frac{c^3}{GI_0}\right)\left(\frac{2GM}{c^2r_0}\right)\\ &\quad\times\frac{1+\sum_{k=1}^{n}(2k+1)\,Q_{2k}P_{2k}\,(0)}{\sum_{k=1}^{n}2\,(2k-1)\,M_{2k}C_{2k}^{(-1/2)}\,(0)},\end{aligned}\tag{7.5}$$

the velocity is given by Eq. (5.41), here repeated,

$$\begin{aligned}&\frac{u_\varphi\,(r_0,\pi/2)}{c}\\ &=-\frac{\left(\frac{c^3}{GI_0}\right)\left(\frac{2GM}{c^2r_0}\right)\frac{1}{n}\left(1+\sum_{k=1}^{n}(2k+1)\,Q_{2k}\,P_{2k}(0)\right)}{1+\sqrt{1+2\left(\frac{c^3}{GI_0}\right)^2\left(\frac{2GM}{c^2r_0}\right)\frac{1}{n}\left(1+\sum_{k=1}^{n}(2k+1)\,Q_{2k}\,P_{2k}(0)\right)}}.\end{aligned}\tag{7.6}$$

An infinite number of terms is needed to give an exact representation of the velocity at all points of the fluid-vacuum interface. Figure 6 shows that large oscillations occur notably near the poles of the oblate spheroid. Nevertheless, the velocity at the equatorial edge can be calculated with sufficient

precision using the ten multipoles expansion listed in Table 1. A plot of the rotation velocity at the edge, as a function of the normalized mass $GM/(c^2 r_0)$ and of the total current parameter GI_0/c^3, is shown in Fig. 8. The maximum velocity is obtained in the limit when $GI_0/c^3 \to 0$, but this does not mean that the gravitomagnetic effects are neglected. The external constant GM flux, related to the total current I_0, may have a very low value, but it extends to infinity. The boundary conditions fixed by the virtual casing define the distribution both of the scalar potential and of the flux function in the internal region, setting the requirements for equilibrium. The gravitomagnetic braking effect increases with the constant external flux, leading to a decrease in the rotation velocity at the boundary, but this is the same as rotating the reference frame (a transformation of the Larmor gravitomagnetic field).

The rotation flow velocity at an arbitrary position along the boundary is given by Eq. (5.27) with M_{2k} replaced by Eq. (5.40)

$$
\begin{aligned}
\frac{u_\varphi\left[r\left(\theta\right),\theta\right]}{c} = & -\frac{\left(\frac{c^3}{GI_0}\right)\left(\frac{2GM}{c^2 r_0}\right)}{1+\sqrt{1+2\left(\frac{c^3}{GI_0}\right)^2\left(\frac{2GM}{c^2 r_0}\right)\frac{1}{n}\left(1+\sum_{k=1}^{n}\left(2k+1\right)Q_{2k}P_{2k}\left(0\right)\right)}} \\
& \times\left\{r\left(\theta\right)\rho_0'\left[r\left(\theta\right)\right]\left[1+\sum_{k=1}^{n}\left(2k+1\right)Q_{2k}\left(\frac{r_0}{r\left(\theta\right)}\right)^{2k}P_{2k}\left(\cos\theta\right)\right]\right. \\
& \left.-\frac{e^2\rho_0 r\left(\theta\right)^2}{r_0^2}\left[\cos 2\theta+\sum_{k=1}^{n}\left(2k+1\right)Q_{2k}\left(\frac{r_0}{r\left(\theta\right)}\right)^{2k}\left[2\cos\theta P_{2k+1}\left(\cos\theta\right)-P_{2k}\left(\cos\theta\right)\right]\right]\right\} \\
& \times\left\{\frac{1}{n}\sum_{k=1}^{n}\left(\frac{r_0}{r\left(\theta\right)}\right)^{2(k-1)}\left[r\left(\theta\right)\rho_0'\left[r\left(\theta\right)\right]\frac{\left(2k-1\right)C_{2k}^{(-1/2)}\left(\cos\theta\right)}{C_{2k}^{(-1/2)}\left(0\right)\sin\theta}\right.\right. \\
& \left.\left.-\frac{e^2\rho_0 r\left(\theta\right)^2}{r_0^2}\left(\frac{\left(2k-1\right)\cos 2\theta\, C_{2k}^{(-1/2)}\left(\cos\theta\right)}{C_{2k}^{(-1/2)}\left(0\right)\sin\theta}+\frac{\sin 2\theta P_{2k-1}\left(\cos\theta\right)}{C_{2k}^{(-1/2)}\left(0\right)}\right)\right]\right\}^{-1}.
\end{aligned}
\tag{7.7}
$$

This expression has $2(n-1)$ singularities in the interval $0 < \theta < \pi$ forming a sequence of doublet functions, as shown in the right-hand panel of Fig. 9. The singularities are associated with the finite number of terms in the series and respective gravitomagnetic field oscillations, which should disappear for $n \to \infty$. Figure 9 shows that the scalar potential at the boundary can be approximated by a smooth interpolation function free of oscillations. This interpolation corresponds to half-value of $\phi_{\text{part}}\left[r\left(\theta\right),\theta\right]$ shown in the right-hand panel of Fig. 6 (the dashed line). Figure 9 also shows that the fluid velocity $u_\varphi\left[r\left(\theta\right),\theta\right]$ is approximately given by the envelope of the family of doublet functions taken with the same sign (this presumably gives the exact value in the limit $n \to \infty$). This problem is associated with the calculation of the tangential component of the gravitomagnetic field at the boundary, using a sum of multipole components M_{2k}. These multipole components can be calculated unambiguously in terms of integrals of the mass current density, as indicated by Eq. (5.16). However, the inverse calculation is ill-posed, since an arbitrary periodic function of θ can be added to the integrand without changing the values of M_{2k} (the same problem occurs if the mass density is calculated in terms of the multipole components Q_{2k}). The smoothed out boundary profiles can also be obtained using a Gauss filtering process, which removes the small wavelength oscillations.

Now, using the approximate values of $\phi_{\text{int}}[r(\theta),\theta]$ and $u_\varphi[r(\theta),\theta]$ at the boundary, the fluid velocity $u_\varphi\left(r,\theta\right)$ and the flux function $\psi_{\text{int}}\left(r,\theta\right)$ distributions inside the fluid can be calculated using Eqs. (4.13). Figure 10 shows simplified profiles of the internal scalar potential and of the fluid rotation velocity. The normalized total mass has been reduced to $GM/(c^2 r_0) = 0.03228$ (a factor of ten with respect to the previous figures of the scalar potential), and the normalized total current is $GI_0/c^3 = 10^{-3}$, which corresponds to an effectively small value. The mass reduction decreases the scalar potential well by a factor of ten (cf. Fig. 7), reducing the maximum rotation velocity at the vortex center to values marginally within the weak relativistic approximation $\boldsymbol{u}\cdot\boldsymbol{u} \ll c^2$.

Figures 11 and 12 show detailed density plots of the internal scalar potential $\phi_{\text{int}}\left(r,\theta\right)$, and both of the fluid rotation velocity $u_\varphi\left(r,\theta\right)$ and internal flux function $\psi_{\text{int}}\left(r,\theta\right)$, respectively. These figures correspond to the reduced total mass $GM/(c^2 r_0) = 0.03228$ and very small total current $GI_0/c^3 \to 0$. They show the equilibrium of a rotational vortex with increasing velocity towards the center. Nevertheless, the velocity attains finite values at the axis of rotation. This behavior differs from the rotational rigid rotor and irrotational vortices solutions, which have vanishing and infinite

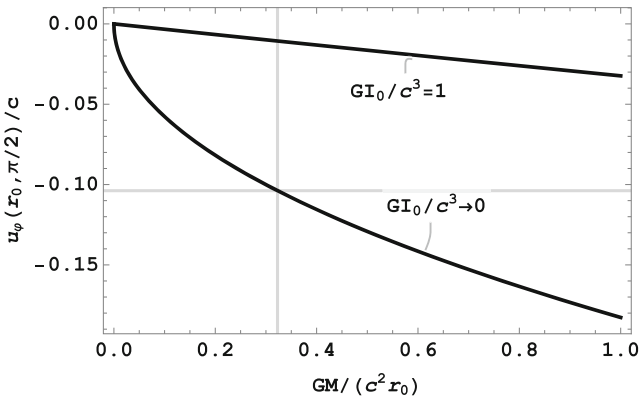

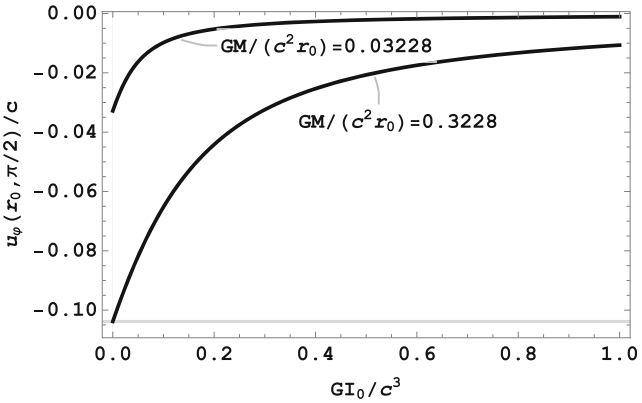

Fig. 8 Rotation velocity at the equatorial edge of an oblate spheroid represented by the set of geometrical parameters listed in Table 1. The left-hand panel shows the velocity variation as a function of the normalized mass contained in the system, for two values of the total current parameter. The vertical line indicates the mass $GM/(c^2r_0) = 0.3228$ for the Gaussian mass density profile described in the text. The right-hand panel shows the velocity variation as a function of the total current parameter, for two values of the normalized mass. These figures clearly show the braking action of the gravitomagnetic field

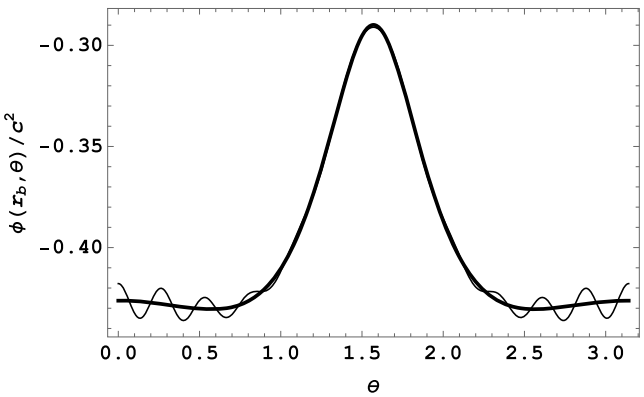

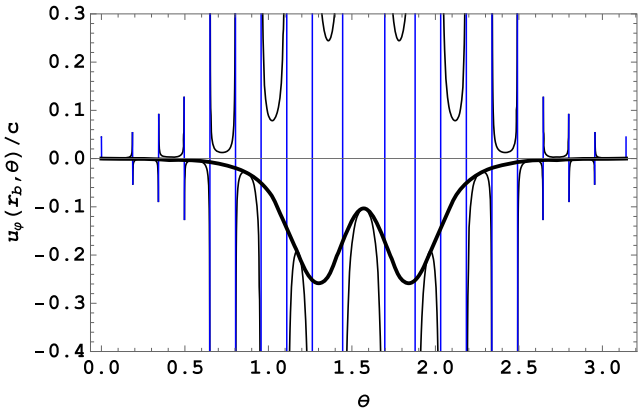

Fig. 9 Interpolated scalar potential and velocity at the fluid-vacuum interface. The left-hand panel compares an interpolation of the internal scalar potential (thick line) with the external potential (thin line), at the boundary. The right-hand panel shows the interpolation of the fluid velocity (thick line) to the envelope of the family of doublet functions (thin line) associated with the oscillations in the truncated series expansions. These figures correspond to a normalized total mass $GM/(c^2r_0) = 0.3228$ and a normalized total current $GI_0/c^3 = 10^{-3}$ (effectively zero) for the Gaussian mass density profile described in the text. The same total mass is used in Figs. 4, 5, 6 and 7

rotational velocities at the axis, respectively. This characterizes a rotational flow with shear, in accordance with the classic observations by Oort [58]. The scalar potential of the oblate spheroidal well deepens at two angular positions which are symmetric with respect to the equatorial plane, so that the velocity forms a thick symmetric hourglass shaped ring with increasing intensity towards the center. The flux function has a maximum around the equatorial plane, dropping to zero at the axis of rotation.

Figure 13 is similar to Fig. 10, showing the effect of an increase in the normalized total current to $GI_0/c^3 = 1$ while maintaining the normalized total mass $GM/(c^2r_0) = 0.03228$ unchanged. The scalar potential does not change, but the rotation velocity at the fluid-vacuum interface is significantly reduced due to the braking action of the external gravitomagnetic field. Figure 14 shows that small changes occur in the internal distributions both of the rotation velocity and of the flux function due to the change in the rotation velocity at the interface, according to the conservation of energy equation (4.12).

8 Comments and conclusions

In this paper, a detailed equilibrium solution for a large scale gravitational system was developed in the extended gravitoelectromagnetic framework. The system was considered as a rotating fluid dust, with negligible pressure effects. Assuming stationary conditions and azimuthal symmetry, the force balance equation was written in the form of a field equation relating the gravitoelectric scalar potential ϕ and the gravit-

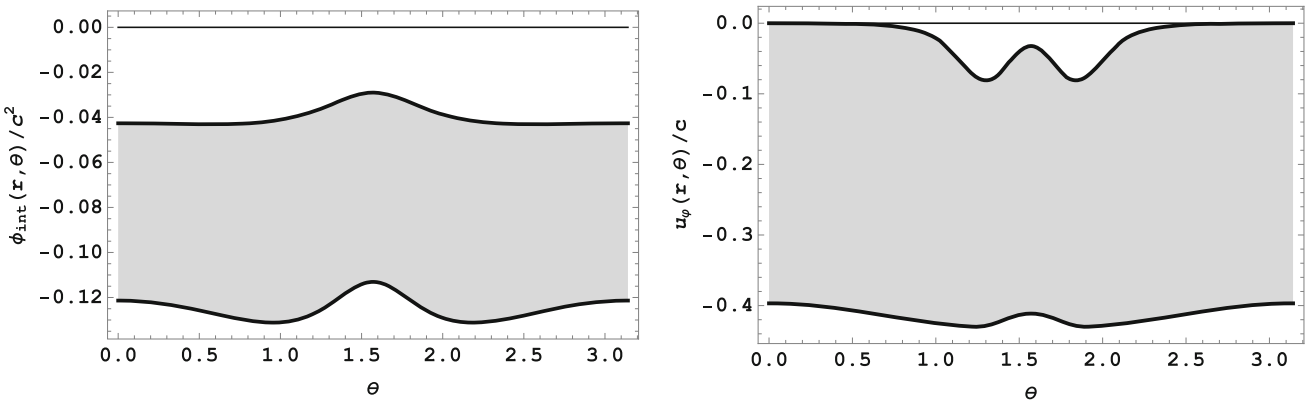

Fig. 10 The left-hand panel shows the scalar potential profile at the fluid-vacuum interface $r\,(\theta)$ (upper line) and along the axis $r = 0$ (bottom line). The shaded area indicates the fluid region. The right-hand panel shows the rotation velocity profiles at the same radial positions. The rotation profile clearly shows where symmetrical current rings form inside the fluid. These figures correspond to a normalized total mass $GM/(c^2 r_0) = 0.03228$ and a normalized total current $GI_0/c^3 = 10^{-3}$ for the Gaussian mass density profile described in the text. Note that the mass is ten times less that the mass used in Fig. 9, to avoid ultra-relativistic velocities at the vortex center

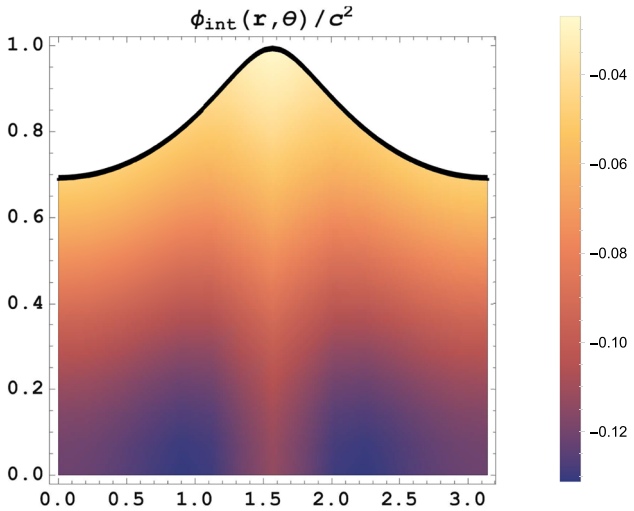

Fig. 11 Density plot of the internal scalar potential corresponding to a normalized total mass $GM/(c^2 r_0) = 0.03228$ and a normalized total current $GI_0/c^3 = 10^{-3}$ for the Gaussian mass density profile described in the text. The horizontal axis displays the polar angle $0 \le \theta \le \pi$, and the vertical axis displays the normalized radial distance $0 \le r/r_0 \le 1$

omagnetic flux function ψ. Furthermore, Maxwell's source equations relate ϕ and ψ to the mass density ρ and to the mass current density $j_\varphi = \rho u_\varphi$, respectively. The field equation describes the nonlocal interactions, while the source equations describe the local exchange of energy and momentum between field and matter.

The boundary conditions at the fluid-vacuum interface were taken into account using the Helmholtz decomposition of the combined field formed by a sum of the gravitoelectric and gravitomagnetic fields. This decomposition clearly separates the particular solutions, given by volume integrals over the sources, from the homogeneous solutions, given by surface integrals of the fields at the fluid-vacuum interface. Equivalent surface mass and surface mass current densities were defined in terms of the normal component of the gravitoelectric field and of the tangential component of the gravitomagnetic field, respectively, just outside the interface. Then, the virtual casing principle was used to relate the particular solutions to multipole expansions of the fields in the vacuum region. The homogeneous solutions are related to these same multipole expansions by means of the surface densities. The force balance equation links the rotation velocity u_φ to the internal ϕ and ψ fields, given by the sum of the particular and homogeneous solutions.

Using a hydro-gravitomagnetic Cauchy invariant it was demonstrated that the total canonical circulation is null. Hence, the flux function ψ is simply related to the fluid velocity u_φ. Then, the force balance allows to derive the equation of energy conservation, which gives the rotation velocity in terms of the internal scalar potential and the respective boundary conditions. The Cauchy invariant expresses the exchange of fluid and field vorticities in the internal region. The fluid vorticity vanishes at the fluid-vacuum interface, but the field vorticity in the vacuum region is maintained by the

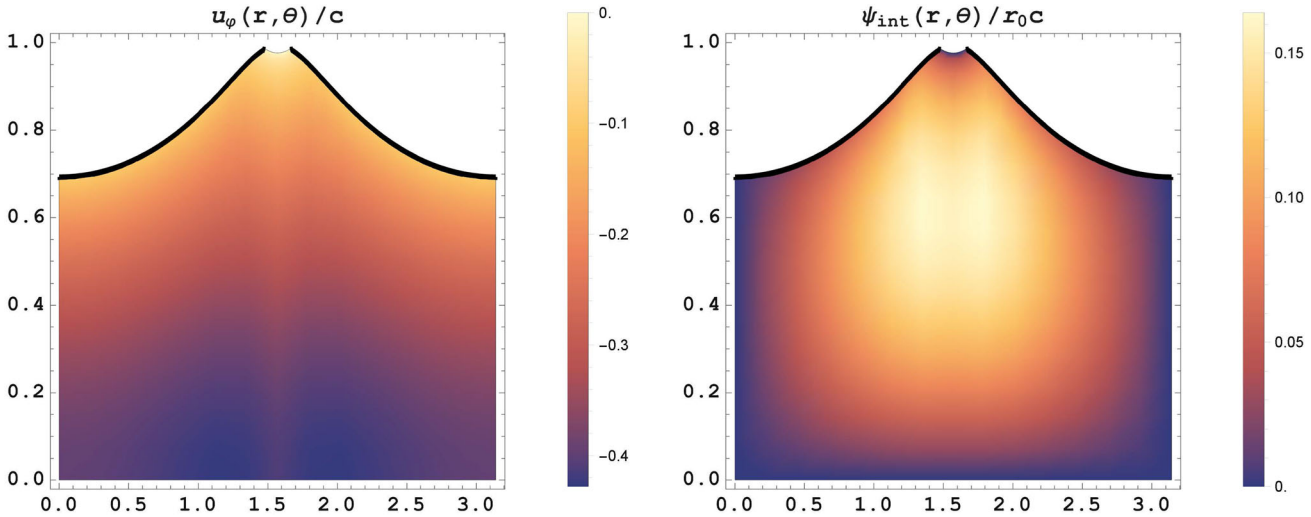

Fig. 12 Density plots of the rotating velocity and of the internal flux function corresponding to a normalized total mass $GM/(c^2 r_0) = 0.03228$ and a normalized total current $GI_0/c^3 = 10^{-3}$ for the Gaussian mass density profile described in the text. The horizontal axis displays the polar angle $0 \leq \theta \leq \pi$, and the vertical axis displays the normalized radial distance $0 \leq r/r_0 \leq 1$

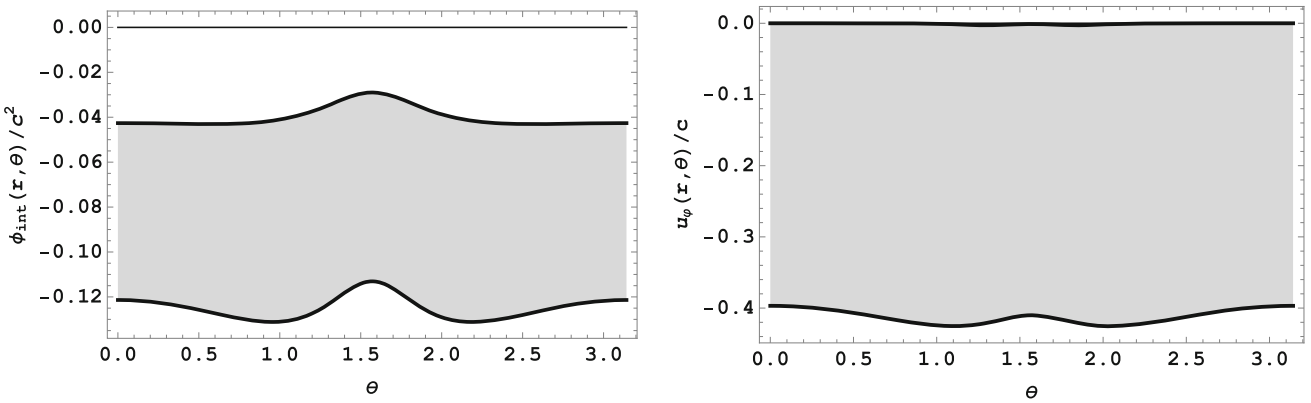

Fig. 13 The left-hand panel shows the scalar potential profile at the fluid-vacuum interface $r(\theta)$ (upper line) and along the axis $r = 0$ (bottom line). The shaded area indicates the fluid region. The right-hand panel shows the rotation velocity profiles at the same radial positions. These figures correspond to the a normalized total mass $GM/(c^2 r_0) = 0.03228$ and a normalized total current $GI_0/c^3 = 1$ for the Gaussian mass density profile described in the text. Note that the mass is ten times less that the mass used in Fig. 9, to avoid ultra-relativistic velocities at the vortex center. In comparison with Fig. 10 there is no change in the scalar potential profile, but the rotation velocity at the fluid-vacuum interface drops to very low values

rotating fluid, or vice-versa. The energy conservation clearly shows that the gravitomagnetic field does not work directly in stationary conditions, but reduces the rotation velocity at the fluid boundary by means of a braking action. This reduction at the boundary modifies the internal velocity distribution. The gravitomagnetic field reduces the internal gravitational pull, making possible the polar equilibrium, and reduces the rotation velocity, consequently reducing the Coriolis effect. This same actions define the correct value of the anomalous perihelion shift in planetary motion.

Combining the field and source equations, a convolution type volume integral over the mass density and the rotation velocity was equated to the surface integral, at the fluid-vacuum interface, of terms involving the rotation velocity and the equivalent surface densities. Integrability considerations define the rotation velocity at the interface as the ratio between the equivalent source densities.

Since the form of the fluid-vacuum interface is part of the solution, two classes of problems can be distinguished, namely, the fixed and free-boundary problems. In order to simplify the calculations, the system of integro-differential equations describing the equilibrium of the gravitationally contained fluid was specialized to the case of rotating oblate spheroids with fixed eccentricity. Further geometrical and

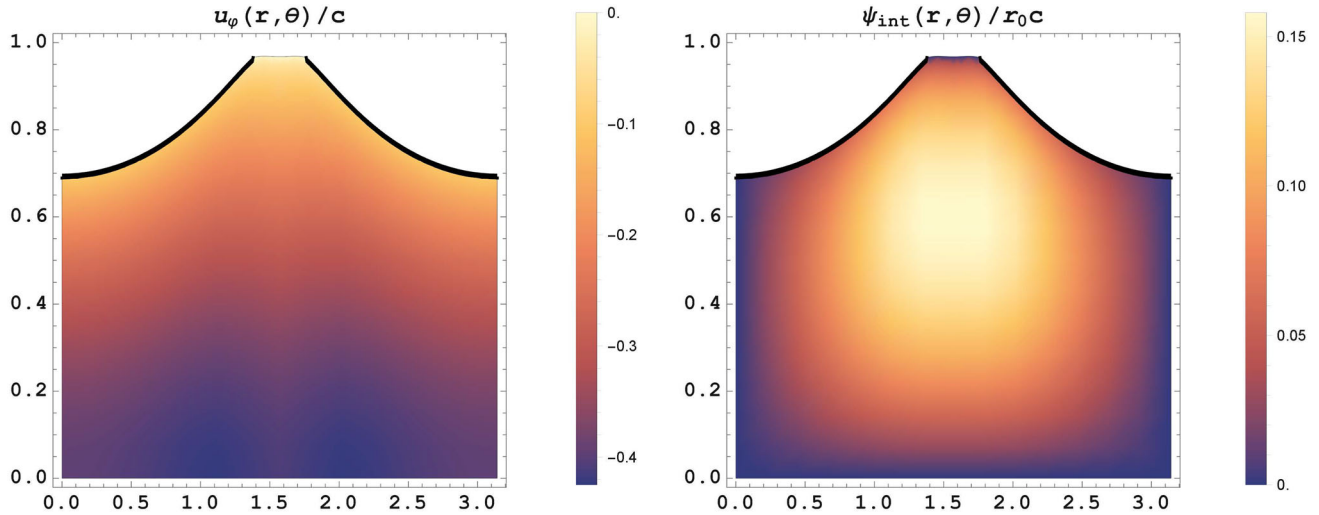

Fig. 14 Density plot of the rotating velocity and of the internal flux function corresponding to a normalized total mass $GM/(c^2r_0) = 0.03228$ and a normalized total current $GI_0/c^3 = 1$ for the Gaussian mass density profile described in the text. The horizontal axis displays the polar angle $0 \leq \theta \leq \pi$, and the vertical axis displays the normalized radial distance $0 \leq r/r_0 \leq 1$. The braking action of the GM field at the fluid-vacuum interface results in more diffuse velocity and internal flux function profiles. The imperfect representations at the edge are a consequence of truncation errors

boundary conditions at the rotation axis put a constraint on the mass density profile, linking the eccentricity to the gravitoelectric multipole coefficients. These conditions also give a relation between the rotation velocity, at the equatorial edge of the fluid region, and both the gravitoelectric and gravitomagnetic multipole coefficients. Finally, the continuity condition of the flux function at the fluid-vacuum interface gives the value of each gravitomagnetic multipole coefficient in terms of the total mass, the total mass current, and a sum of all gravitoelectric multipole coefficients. In this way, the total current can be expressed non-linearly in terms of the total mass, the sum of the gravitoelectric multipole coefficients, and the rotation velocity at the equatorial edge.

Using the relation between total current, total mass, and multipole coefficients, it is possible to make simple estimates assuming that the total mass is distributed, for example, over a circular ring, a disk or a spherical shell. These distributions modify the moment of inertia of the system, but give the squared rotation velocity at the edge in terms of a cubic equation with coefficients depending on the total mass and the sum of multipole coefficients. Further simplifications show that these results are consistent with the Tully–Fisher relation and the Virginia Trimble correlations. Simple dimensional analyses provide the same result.

In order to make a complete equilibrium calculation it is necessary to provide a reasonable radial mass density profile to the rotating spheroid. A monotonic Gaussian profile was implemented and tested for varying values both of the total mass and the total current. The problem has two free parameters that set the scales, namely, the minimum radius r_0 completely enclosing the mass distribution, and the reference mass density ρ_0. For a given mass density profile the equilibrium is completely defined in terms of the normalized Schwarzschild radius $2GM/c^2r_0$ and the normalized current parameter GI_0/c^3. The detailed calculations show that the equilibrium is characterized by a rotational vortex with shear. The rotation velocity forms a thick symmetric hourglass shaped ring. The velocity increases toward the center, but attains finite values at the axis, constituting an intermediate solution between a rigid rotor and an irrotational vortex.

The gravitoelectric multipole components were calculated in terms of a Fourier cosine expansion of the Dirichlet boundary condition for the scalar potential (the virtual casing principle). This direct calculation requires some precision but is easily performed. Unfortunately, the coefficients converge slowly to zero, with alternating signs. Therefore, a large number of terms is necessary to reduce the gravitational potential oscillations just outside the fluid-vacuum interface, particularly near the axis of rotation. On the other hand, the inverse calculation of the gravitomagnetic field in terms of the gravitomagnetic multipole components is ill-posed. The zeros of the mass current density at the interface produce a sequence of doublet functions in the calculation of the rotation velocity. These doublets reflect discontinuous changes in the direction of rotation at the surface where the velocity must drop to zero. This calculation needs some regularization and requires further studies.

The model can be applied to various configurations by changing the radial mass density profile. A peaked profile combined with a slowly decaying term reduces the mass in

the large outer region. However, a disk-like configuration requires a more complex spectral representation of the mass density distribution, and consequently of the fluid-vacuum interface. It would be interesting to test the limits of a very peaked profile at the center and of an almost flat profile, as well as the introduction of a very large scale external potential. In retrospect, it is noted that the rotation velocity was assumed to vanish at the extreme axial points of the oblate spheroid fluid-vacuum interface, leading to a vortex configuration with increasing velocity towards the center. Conceivably, if the velocity takes a finite value at these extreme points, a similar solution can be determined, with decreasing velocity towards the center in correspondence with the rotation of galaxies. These studies and the reinstatement of the full relativistic fluid inertia are postponed for future work.

According to the virial theorem, twice the kinetic energy in a pressureless system is contained by the internal negative gravitational energy, plus the back pressure exerted by the external fields on the fluid-vacuum interface. The matter vortex in the present problem is partially confined by the internal gravitoelectric and gravitomagnetic fields energy. The external gravitoelectric field contributes with a negative pressure that decays away since the gravitational potential ϕ was assumed to vanish at infinity. The energy stored in the gravitoelectric field is controlled by the normalized Schwarzschild radius $2GM/c^2r_0$. Besides the decaying contributions, the external gravitomagnetic field has a constant circulation associated with the total mechanical momentum of the mass distribution. This circulation is controlled by the normalized total current parameter GI_0/c^3. If the braking action of the external gravitomagnetic field increases significantly, the velocity at the entire boundary essentially vanishes, so that the internal velocity increase towards the center is controlled by the drop in the equatorially symmetric scalar potential well. Nevertheless, the internal geometry defined by the force balance is essentially maintained. The change in circulation is equivalent to a rotation of the coordinates, in accordance with Larmor's theorem and Mach's principle.

Acknowledgements This work was supported by a grant provided by the *Programa de Capacitação Institucional: Diretoria de Pesquisa e Desenvolvimento/Comissão Nacional de Energia Nuclear (CNEN).*

Data Availability Statement This manuscript has no associated data or the data will not be deposited. [Authors' comment: This is a theoretical paper for which no data has been generated.]

Funded by SCOAP[3].

Appendix A: Gravitoelectromagnetic field in the external region

In the external region the scalar potential satisfies Laplace's equation (homogeneous solutions)

$$r^2\nabla\cdot\nabla\phi\,(r,\theta) = \frac{\partial}{\partial r}\left(r^2\frac{\partial\phi\,(r,\theta)}{\partial r}\right) + \frac{1}{\sin\theta}\frac{\partial}{\partial\theta}\left(\sin\theta\frac{\partial\phi\,(r,\theta)}{\partial\theta}\right)=0, \tag{A1}$$

and the flux function satisfies Grad-Shafranov's equation without sources

$$r^4\sin^2\theta\nabla\cdot\left(\frac{\nabla\psi\,(r,\theta)}{r^2\sin^2\theta}\right) = r^2\frac{\partial^2\psi\,(r,\theta)}{\partial r^2} + \sin\theta\frac{\partial}{\partial\theta}\left(\frac{1}{\sin\theta}\frac{\partial\psi\,(r,\theta)}{\partial\theta}\right)=0. \tag{A2}$$

The general homogeneous solutions are given in terms of Legendre polynomials for ϕ, and in terms of Gegenbauer polynomials for ψ

$$\begin{cases}\phi\,(r,\theta) = \sum_{k=0}^{n}\left(a_kr^k+b_kr^{-(k+1)}\right)P_k\,(\cos\theta)\\ \psi\,(r,\theta) = \sum_{k=0}^{n}\left(c_kr^k+d_kr^{1-k}\right)C_k^{(-1/2)}\,(\cos\theta)\end{cases} \tag{A3}$$

Assuming equatorial symmetry and finite solutions at $r\to\infty$

$$\begin{cases}\phi_{\text{ext}}\,(r,\theta) = a_0+\sum_{k=0}^{n}b_{2k}r^{-(2k+1)}P_{2k}\,(\cos\theta)\\ \psi_{\text{ext}}\,(r,\theta) = c_0+\sum_{k=1}^{n}d_{2k}r^{-(2k-1)}C_{2k}^{(-1/2)}\,(\cos\theta)\end{cases} \tag{A4}$$

These homogeneous solutions automatically satisfy the field equation (2.15) in vacuum. They provide the juncture conditions along the fluid-vacuum interface, that is, the requirement that the potential $\phi\,(r,\theta)$ and the flux function $\psi\,(r,\theta)$ be continuous across the interface while attaining constant values at $r\to\infty$. Taking $a_0=0$ for vanishing potential at infinity (this choice characterizes the class of vortex solutions analyzed in the present paper) and defining a reference radial distance r_0 (usually the radius of the smallest sphere completely enclosing the mass density ρ), the expansion of

$\phi_{\text{ext}}(r,\theta)$ in Legendre polynomials can be written in the standard multipole expansion form

$$\phi_{\text{ext}}(r,\theta) = -\frac{GM}{r}\left(1+\sum_{k=1}^{n} Q_{2k}\left(\frac{r_0}{r}\right)^{2k} P_{2k}(\cos\theta)\right), \tag{A5}$$

where the following replacements were introduced

$$b_0 = -GM, \quad b_{2k} = b_0 r_0^{2k} Q_{2k} \quad \text{and} \quad Q_0 = 1 \text{ (monopole)} \tag{A6}$$

Just outside the fluid-vacuum interface the surface integral for $\phi_{\text{int}}(r,\theta)$ in Eq. (3.10) corresponds to the total volume integral in the internal region (with inverted sign), leading to the relation between the volume integral and the multipole expansion on the outside face of S (note that $\boldsymbol{r}(\theta)$ designates a position on the fluid-vacuum interface)

$$\int_V \frac{\rho(r',\theta')}{|\boldsymbol{r}(\theta)-\boldsymbol{r}'|}dV' = \frac{2M}{r(\theta)} \times\left(1+\sum_{k=1}^{n} Q_{2k}\left(\frac{r_0}{r(\theta)}\right)^{2k} P_{2k}(\cos\theta)\right). \tag{A7}$$

In the present formulation the expansions are exactly valid in the vacuum region. They are not limited by the large distance condition $r > r_0$, giving an exact representation of the fluid-vacuum interface.

Introducing the further replacements

$$c_0 = -\psi_0 \quad , \quad d_{2k} = d_2 r_0^{2k-1} M_{2k} \quad \text{and} \quad d_2 = -\psi_0, \tag{A8}$$

the flux function can also be written in the form of a gravitomagnetic multipole expansion

$$\psi_{\text{ext}}(r,\theta) = -\psi_0\left(1+\sum_{k=1}^{n} M_{2k}\left(\frac{r_0}{r}\right)^{2k-1} C_{2k}^{(-1/2)}(\cos\theta)\right), \tag{A9}$$

so that, on the outside face of S,

$$\int_V \frac{j_\varphi(r',\theta')}{|\boldsymbol{r}(\theta)-\boldsymbol{r}'|}dV' = \frac{2r_0 I_0}{r(\theta)\sin\theta}\left(1+\sum_{k=1}^{n} M_{2k}\left(\frac{r_0}{r(\theta)}\right)^{2k-1} C_{2k}^{(-1/2)}(\cos\theta)\right), \tag{A10}$$

where $I_0 = c^2\psi_0/(Gr_0)$ is the total mass current associated with the reference flux function ψ_0.

Appendix B: Gravitoelectromagnetic field in the internal region

The scalar potential and the flux function are given in the internal fluid region by equations (3.10). For axisymmetric systems the integration over the angle φ in polar spherical coordinates gives

$$\int_0^{2\pi}\frac{d\varphi}{|\boldsymbol{r}-\boldsymbol{r}'|} = \frac{4K\left[m\left(r,r';\theta,\theta'\right)\right]}{\sqrt{r^2+r'^2-2rr'\cos(\theta-\theta')}}, \tag{B1}$$

so that the integrals (3.10) can be written in explicit form

$$\begin{cases} \phi_{\text{int}}(r,\theta) = -G\int_0^{\pi}\int_0^{r(\theta')} \\ \quad \frac{4\rho(r',\theta')K\left[m\left(r,r';\theta,\theta'\right)\right]r'^2\sin\theta'}{\sqrt{r^2+r'^2-2rr'\cos(\theta-\theta')}}dr'd\theta' \\ \quad -G\int_0^{\pi}\frac{4\sigma\left[r(\theta'),\theta'\right]K\left[m\left(r,r(\theta');\theta,\theta'\right)\right]r(\theta')^2\sin\theta'}{\sqrt{r^2+r(\theta')^2-2rr(\theta')\cos(\theta-\theta')}}d\theta' \\ \psi_{\text{int}}(r,\theta) = -\frac{Gr\sin\theta}{c^2}\int_0^{\pi}\int_0^{r(\theta')} \\ \quad \frac{4j_\varphi(r',\theta')K\left[m\left(r,r';\theta,\theta'\right)\right]r'^2\sin\theta'}{\sqrt{r^2+r'^2-2rr'\cos(\theta-\theta')}}dr'd\theta' - \frac{Gr\sin\theta}{c^2} \\ \quad \int_0^{\pi}\frac{4K_\varphi\left[r(\theta'),\theta'\right]K\left[m\left(r,r(\theta');\theta,\theta'\right)\right]r(\theta')^2\sin\theta'}{\sqrt{r^2+r(\theta')^2-2rr(\theta')\cos(\theta-\theta')}}d\theta' \end{cases} \tag{B2}$$

where $K(m)$ denotes the complete elliptic integral of the first kind as a function of the parameter $-1 < m < 1$,

$$m\left(r,r';\theta,\theta'\right) = -\frac{4rr'\sin\theta\sin\theta'}{\sqrt{r^2+r'^2-2rr'\cos(\theta-\theta')}}, \tag{B3}$$

with $0 \le r \le r(\theta)$, and $r(\theta)$ corresponding to a radial position along the fluid-vacuum interface. The gravitoelectromagnetic field $\boldsymbol{H} = -\nabla\phi + c\nabla\times\boldsymbol{A}$ is given in terms of the gradient of $\phi(r,\theta)$ and the curl of $\boldsymbol{A}(r,\theta)$ in spherical coordinates

$$\begin{cases} \nabla\phi(r,\theta) = \frac{\partial\phi}{\partial r}\widehat{\boldsymbol{r}} + \frac{1}{r}\frac{\partial\phi}{\partial\theta}\widehat{\boldsymbol{\theta}} \\ \nabla\times\boldsymbol{A} \quad = \frac{1}{r^2\sin\theta}\left(\frac{\partial\psi}{\partial\theta}\widehat{\boldsymbol{r}} - r\frac{\partial\psi}{\partial r}\widehat{\boldsymbol{\theta}}\right) \end{cases} \tag{B4}$$

where

$$\frac{\partial\phi_{\text{int}}}{\partial r}=\frac{G}{r}\int_0^{\pi}\int_0^{r(\theta')}\frac{2\rho\left(r',\theta'\right)r'^2\sin\theta'}{\sqrt{r^2+r'^2-2rr'\cos\left(\theta-\theta'\right)}}\left(\frac{\left(r^2-r'^2\right)E\left[m\left(r,r';\theta,\theta'\right)\right]}{r^2+r'^2-2rr'\cos\left(\theta+\theta'\right)}+K\left[m\left(r,r';\theta,\theta'\right)\right]\right)dr'd\theta'$$
$$+\frac{G}{r}\int_0^{\pi}\frac{2\sigma\left[r\left(\theta'\right),\theta'\right]r\left(\theta'\right)^2\sin\theta'}{\sqrt{r^2+r\left(\theta'\right)^2-2rr\left(\theta'\right)\cos\left(\theta-\theta'\right)}}\left(\frac{\left(r^2-r\left(\theta'\right)^2\right)E\left[m\left(r,r\left(\theta'\right);\theta,\theta'\right)\right]}{r^2+r\left(\theta'\right)^2-2rr\left(\theta'\right)\cos\left(\theta+\theta'\right)}+K\left[m\left(r,r\left(\theta'\right);\theta,\theta'\right)\right]\right)d\theta', \tag{B5}$$

$$\frac{\partial\phi_{\text{int}}}{\partial\theta}=-\frac{G}{\sin\theta}\int_0^{\pi}\int_0^{r(\theta')}\frac{2\rho\left(r',\theta'\right)r'^2\sin\theta'}{\sqrt{r^2+r'^2-2rr'\cos\left(\theta-\theta'\right)}}$$
$$\times\left(\frac{\left[\left(r^2+r'^2\right)\cos\theta-2rr'\cos\theta'\right]E\left[m\left(r,r';\theta,\theta'\right)\right]}{r^2+r'^2-2rr'\cos\left(\theta+\theta'\right)}-\cos\theta\,K\left[m\left(r,r';\theta,\theta'\right)\right]\right)dr'd\theta'$$
$$-\frac{G}{\sin\theta}\int_0^{\pi}\frac{2\sigma\left[r\left(\theta'\right),\theta'\right]r\left(\theta'\right)^2\sin\theta'}{\sqrt{r^2+r\left(\theta'\right)^2-2rr\left(\theta'\right)\cos\left(\theta-\theta'\right)}}$$
$$\times\left(\frac{\left[\left(r^2+r\left(\theta'\right)^2\right)\cos\theta-2rr\left(\theta'\right)\cos\theta'\right]E\left[m\left(r,r\left(\theta'\right);\theta,\theta'\right)\right]}{r^2+r\left(\theta'\right)^2-2rr\left(\theta'\right)\cos\left(\theta+\theta'\right)}-\cos\theta\,K\left[m\left(r,r\left(\theta'\right);\theta,\theta'\right)\right]\right)d\theta', \tag{B6}$$

$$\frac{\partial\psi_{\text{int}}}{\partial r}=\frac{G\sin\theta}{c^2}\int_0^{\pi}\int_0^{r(\theta')}\frac{2j_{\varphi}\left(r',\theta'\right)r'^2\sin\theta'}{\sqrt{r^2+r'^2-2rr'\cos\left(\theta-\theta'\right)}}\left(\frac{\left(r^2-r'^2\right)E\left[m\left(r,r';\theta,\theta'\right)\right]}{r^2+r'^2-2rr'\cos\left(\theta+\theta'\right)}-K\left[m\left(r,r';\theta,\theta'\right)\right]\right)dr'd\theta'$$
$$+\frac{G\sin\theta}{c^2}\int_0^{\pi}\frac{2K_{\varphi}\left[r\left(\theta'\right),\theta'\right]r\left(\theta'\right)^2\sin\theta'}{\sqrt{r^2+r\left(\theta'\right)^2-2rr\left(\theta'\right)\cos\left(\theta-\theta'\right)}}\left(\frac{\left(r^2-r\left(\theta'\right)^2\right)E\left[m\left(r,r\left(\theta'\right);\theta,\theta'\right)\right]}{r^2+r\left(\theta'\right)^2-2rr\left(\theta'\right)\cos\left(\theta+\theta'\right)}-K\left[m\left(r,r\left(\theta'\right);\theta,\theta'\right)\right]\right)d\theta', \tag{B7}$$

and

$$\frac{\partial\psi_{\text{int}}}{\partial\theta}=-\frac{Gr}{c^2}\int_0^{\pi}\int_0^{r(\theta')}\frac{2j_{\varphi}\left(r',\theta'\right)r'^2\sin\theta'}{\sqrt{r^2+r'^2-2rr'\cos\left(\theta-\theta'\right)}}\left(\frac{\left[\left(r^2+r'^2\right)\cos\theta-2rr'\cos\theta'\right]E\left[m\left(r,r';\theta,\theta'\right)\right]}{r^2+r'^2-2rr'\cos\left(\theta+\theta'\right)}+\cos\theta\,K\left[m\left(r,r';\theta,\theta'\right)\right]\right)dr'd\theta'$$
$$-\frac{Gr}{c^2}\int_0^{\pi}\frac{2K_{\varphi}\left[r\left(\theta'\right),\theta'\right]r\left(\theta'\right)^2\sin\theta'}{\sqrt{r^2+r\left(\theta'\right)^2-2rr\left(\theta'\right)\cos\left(\theta-\theta'\right)}}\left(\frac{\left[\left(r^2+r\left(\theta'\right)^2\right)\cos\theta-2rr'\cos\theta'\right]E\left[m\left(r,r\left(\theta'\right);\theta,\theta'\right)\right]}{r^2+r\left(\theta'\right)^2-2rr\left(\theta'\right)\cos\left(\theta+\theta'\right)}+\cos\theta\,K\left[m\left(r,r\left(\theta'\right);\theta,\theta'\right)\right]\right)d\theta. \tag{B8}$$

Here $E\left(m\right)$ is the complete elliptic integral of the second kind. Accordingly, the skew projection of the combined internal gravitoelectromagnetic field is given by

$$r\left(\boldsymbol{\nabla}\times\widehat{\boldsymbol{\varphi}}\right)\cdot\boldsymbol{H}_{\text{int}}=r\left(\boldsymbol{\nabla}\times\widehat{\boldsymbol{\varphi}}\right)\cdot\left(-\boldsymbol{\nabla}\phi_{\text{int}}+c\boldsymbol{\nabla}\times\boldsymbol{A}_{\text{int}}\right), \tag{B9}$$

where

$$r\left(\boldsymbol{\nabla}\times\widehat{\boldsymbol{\varphi}}\right)\cdot\boldsymbol{\nabla}\phi_{\text{int}}\left(r,\theta\right)=\cot\theta\frac{\partial\phi_{\text{int}}}{\partial r}-\frac{1}{r}\frac{\partial\phi_{\text{int}}}{\partial\theta}=\frac{G}{\sin\theta}\int_0^{\pi}\int_0^{r(\theta')}\frac{4\rho\left(r',\theta'\right)r'^2\sin\theta'\left(r\cos\theta-r'\cos\theta'\right)E\left[m\left(r,r';\theta,\theta'\right)\right]}{\sqrt{r^2+r'^2-2rr'\cos\left(\theta-\theta'\right)}\left[r^2+r'^2-2rr'\cos\left(\theta+\theta'\right)\right]}dr'd\theta'$$
$$+\frac{G}{\sin\theta}\int_0^{\pi}\frac{4\sigma\left[r\left(\theta'\right),\theta'\right]r\left(\theta'\right)^2\sin\theta'\left(r\cos\theta-r\left(\theta'\right)\cos\theta'\right)E\left[m\left(r,r\left(\theta'\right);\theta,\theta'\right)\right]}{\sqrt{r^2+r\left(\theta'\right)^2-2rr\left(\theta'\right)\cos\left(\theta-\theta'\right)}\left[r^2+r\left(\theta'\right)^2-2rr\left(\theta'\right)\cos\left(\theta+\theta'\right)\right]}d\theta', \tag{B10}$$

and

$$
\begin{aligned}
r\left(\nabla\times\widehat{\boldsymbol{\varphi}}\right)\cdot\left(c\nabla\times\boldsymbol{A}_{\text{int}}\right) &= \frac{c}{r^2\sin\theta}\left(\cot\theta\frac{\partial\psi_{\text{int}}}{\partial\theta}+r\frac{\partial\psi_{\text{int}}}{\partial r}\right) = -\frac{G}{cr\sin^2\theta}\int_0^{\pi}\int_0^{r(\theta')}\frac{2j_{\varphi}\left(r',\theta'\right)r'^2\sin\theta'}{\sqrt{r^2+r'^2-2rr'\cos\left(\theta-\theta'\right)}}\\
&\times\left(\frac{\left(r^2\cos 2\theta+r'^2-2rr'\cos\theta\cos\theta'\right)E\left[m\left(r,r';\theta,\theta'\right)\right]}{r^2+r'^2-2rr'\cos\left(\theta+\theta'\right)}+K\left[m\left(r,r';\theta,\theta'\right)\right]\right)dr'd\theta'\\
&-\frac{G}{cr\sin^2\theta}\int_0^{\pi}\frac{2K_{\varphi}\left[r\left(\theta'\right),\theta'\right]r\left(\theta'\right)^2\sin\theta'}{\sqrt{r^2+r\left(\theta'\right)^2-2rr\left(\theta'\right)\cos\left(\theta-\theta'\right)}}\\
&\times\left(\frac{\left(r^2\cos 2\theta+r\left(\theta'\right)^2-2rr\left(\theta'\right)\cos\theta\cos\theta'\right)E\left[m\left(r,r\left(\theta'\right);\theta,\theta'\right)\right]}{r^2+r\left(\theta'\right)^2-2rr\left(\theta'\right)\cos\left(\theta+\theta'\right)}+K\left[m\left(r,r\left(\theta'\right);\theta,\theta'\right)\right]\right)d\theta'.
\end{aligned}
\tag{B11}
$$

Also

$$
\begin{aligned}
\frac{r\left(\nabla\times\widehat{\boldsymbol{\varphi}}\right)\cdot\nabla\psi_{\text{int}}\left(r,\theta\right)}{r\sin\theta} &= \frac{1}{r\sin\theta}\left(\cot\theta\frac{\partial\psi_{\text{int}}}{\partial r}-\frac{1}{r}\frac{\partial\psi_{\text{int}}}{\partial\theta}\right)\\
&= \frac{G}{c^2\sin\theta}\int_0^{\pi}\int_0^{r(\theta')}\frac{4j_{\varphi}\left(r',\theta'\right)r'^2\sin\theta'\left(r\cos\theta-r'\cos\theta'\right)E\left[m\left(r,r';\theta,\theta'\right)\right]}{\sqrt{r^2+r'^2-2rr'\cos\left(\theta-\theta'\right)}\left[r^2+r'^2-2rr'\cos\left(\theta+\theta'\right)\right]}dr'd\theta'\\
&+\frac{G}{c^2\sin\theta}\int_0^{\pi}\frac{4K_{\varphi}\left[r\left(\theta'\right),\theta'\right]r\left(\theta'\right)^2\sin\theta'\left(r\cos\theta-r\left(\theta'\right)\cos\theta'\right)E\left[m\left(r,r\left(\theta'\right);\theta,\theta'\right)\right]}{\sqrt{r^2+r\left(\theta'\right)^2-2rr\left(\theta'\right)\cos\left(\theta-\theta'\right)}\left[r^2+r\left(\theta'\right)^2-2rr\left(\theta'\right)\cos\left(\theta+\theta'\right)\right]}d\theta',
\end{aligned}
\tag{B12}
$$

Using Eqs. (B10) and (B12) the force balance can be written in the form of a two-dimensional integral equation for the fluid velocity $u_{\varphi}\left(r,\theta\right)$ in terms of complete elliptic integrals where the new integrand in the first term of the right-hand side is free of singularities.

$$
\begin{aligned}
&\int_0^{\pi}\int_0^{r(\theta')}\left(1-\frac{u_{\varphi}\left(r,\theta\right)u_{\varphi}\left(r',\theta'\right)}{c^2}\right)\frac{4\rho\left(r',\theta'\right)r'^2\sin\theta'\left(r\cos\theta-r'\cos\theta'\right)E\left[m\left(r,r';\theta,\theta'\right)\right]}{\sqrt{r^2+r'^2-2rr'\cos\left(\theta-\theta'\right)}\left[r^2+r'^2-2rr'\cos\left(\theta+\theta'\right)\right]}dr'd\theta'\\
&= -\int_0^{\pi}\left(\sigma\left[r\left(\theta'\right),\theta'\right]-\frac{u_{\varphi}\left(r,\theta\right)}{c}\frac{K_{\varphi}\left[r\left(\theta'\right),\theta'\right]}{c}\right)\frac{4r\left(\theta'\right)^2\sin\theta'\left(r\cos\theta-r\left(\theta'\right)\cos\theta'\right)E\left[m\left(r,r\left(\theta'\right);\theta,\theta'\right)\right]}{\sqrt{r^2+r\left(\theta'\right)^2-2rr\left(\theta'\right)\cos\left(\theta-\theta'\right)}\left[r^2+r\left(\theta'\right)^2-2rr\left(\theta'\right)\cos\left(\theta+\theta'\right)\right]}d\theta'.
\end{aligned}
\tag{B13}
$$

Appendix C: Integrable and non-integrable singularities

The integrals displayed in Eq. (B2) can be conveniently calculated subtracting out the singularity in the integrand. For example, using the limiting value

$$
\frac{4K\left[m\left(r,r';\theta,\theta'\right)\right]r'^2\sin\theta'}{\sqrt{r^2+r'^2-2rr'\cos\left(\theta-\theta'\right)}}\underset{r'\to r,\theta'\to\theta}{\longrightarrow}-r\ln\left(\theta-\theta'\right)^2,
\tag{C1}
$$

the integral for the homogeneous value of the scalar potential can be written as

$$
\begin{aligned}
\phi_{\text{hom}}\left(r,\theta\right) &= -G\int_0^{\pi}\frac{4\sigma\left[r\left(\theta'\right),\theta'\right]K\left[m\left(r,r\left(\theta'\right);\theta,\theta'\right)\right]r\left(\theta'\right)^2\sin\theta'}{\sqrt{r^2+r\left(\theta'\right)^2-2rr\left(\theta'\right)\cos\left(\theta-\theta'\right)}}d\theta'\\
&= -G\int_0^{\pi}\left(\frac{4\sigma\left[r\left(\theta'\right),\theta'\right]K\left[m\left(r,r\left(\theta'\right);\theta,\theta'\right)\right]r\left(\theta'\right)^2\sin\theta'}{\sqrt{r^2+r\left(\theta'\right)^2-2rr\left(\theta'\right)\cos\left(\theta-\theta'\right)}}+\sigma\left[r\left(\theta\right),\theta\right]r\left(\theta\right)\ln\left(\theta-\theta'\right)^2\right)d\theta'\\
&-2G\sigma\left[r\left(\theta\right),\theta\right]r\left(\theta\right)\left[\pi-\left(\pi-\theta\right)\ln\left(\pi-\theta\right)-\theta\ln\theta\right],
\end{aligned}
\tag{C2}
$$

The integrals in Eq. (B13) contain a non-integrable singularity. The limit for $r'\to r$ gives

$$
\begin{aligned}
&\frac{4r'^2\sin\theta'\left(r\cos\theta-r'\cos\theta'\right)E\left[m\left(r,r';\theta,\theta'\right)\right]}{\sqrt{r^2+r'^2-2rr'\cos\left(\theta-\theta'\right)}\left[r^2+r'^2-2rr'\cos\left(\theta+\theta'\right)\right]}\\
&\underset{r'\to r}{\longrightarrow}\begin{cases}-\dfrac{2\sin\theta}{\theta-\theta'} & \text{if}\quad \theta'<\theta\\ \dfrac{\sin\theta}{\left|\sin\left(\dfrac{\theta-\theta'}{2}\right)\right|} & \text{if}\quad \theta'\geq\theta\end{cases}
\end{aligned}
\tag{C3}
$$

leading to undefined values if integrated over $0 \leq \theta' \leq \pi$. This is not a problem for the integral in the left-hand side of Eq. (B13) since $\rho\left(r', \theta'\right)$ vanishes for $r' \to r\left(\theta'\right)$. However, this singularity indicates that the term between parenthesis in the integrand of the right-hand side of Eq. (B13) must also vanish for $r \to r\left(\theta\right)$, that is,

$$\left(\sigma\left[r\left(\theta\right), \theta\right] - \frac{u_\varphi\left(r\left(\theta\right), \theta\right)}{c} \frac{K_\varphi\left[r\left(\theta\right), \theta\right]}{c}\right) = 0. \qquad \text{(C4)}$$

References

1. F. Zwicky, Die Rotverschiebung von extragalaktischen Nebeln. Helv. Phys. Acta **6**, 110–127 (1933)
2. F. Zwicky, Die Rotverschiebung von extragalaktischen Nebeln. Gen. Relativ. Gravit. **41**, 207–224 (2009)
3. S.M. Faber, J.S. Gallagher, Masses and mass-to-light ratios of galaxies. Ann. Rev. Astron. Astrophys. **17**, 135–187 (1979)
4. S.M. Kent, J.E. Gunn, The dynamics of rich clusters of galaxies. I. The Coma cluster. Astron. J. **87**, 945–971 (1982)
5. L.S. The, S.D.M. White, The mass of the Coma cluster. Astron. J. **92**, 1248–1253 (1986)
6. V.C. Rubin, W.K. Ford Jr., N. Thonnard, Extended rotation curves of high-luminosity spiral galaxies, systematic dynamical properties, Sa → Sc. ApJ **225**, L107–L111 (1978)
7. T.S. van Albada, J.N. Bahcall, K. Begeman, R. Sanscisi, Distribution of dark matter in the spiral galaxy NGC 3198. ApJ **295**, 305–313 (1985)
8. S.M. Kent, Dark matter in spiral galaxies. II. Galaxies with HI rotation curves. Astron. J. **93**, 816–832 (1987)
9. V.C. Rubin, One hundred years of rotating galaxies. PASP **112**, 747–750 (2000)
10. Y. Sofue, V.C. Rubin, Rotation curves of spiral galaxies. arXiv:astro-ph/0010594v3 (2019)
11. P. Bianchini, A.L. Varri, G. Bertin, A. Zocchi, Rotating globular clusters. Ap. J. **772**, 67–86 (2013)
12. M.H. Fabricius et al., Central rotations of Milky Way globular clusters. Ap. J. L. **787**, L26 (2014)
13. H.M. Tovmassian, The rotation of galaxy clusters. Astrophysics **58**, 328–337 (2015)
14. M. Manolopoulou, M. Plionis, Galaxy cluster's rotation. MNRAS **465**, 2616–2633 (2016)
15. P. Bianchini et al., The internal rotation of globular clusters revealed by Gaia DR2. MNRAS **481**, 2125–2139 (2018)
16. G. Bertone, D. Hooper, History of dark matter. Rev. Mod. Phys. **90**, 045002:1-045002:32 (2018)
17. F.I. Cooperstock, S. Tieu, Galactic dynamics via General Relativity: a compilation and new developments. Int. J. Mod. Phys. **22**, 2293–2325 (2007). arXiv:astro-ph/0610370, 2018
18. H. Balasin, D. Grumiller, Non-Newtonian behavior in weak field General Relativity for extended rotating sources. Int. J. Mod. Phys. D **17**, 475–488 (2008)
19. N.S. Magalhaes, F.I. Cooperstock, Mass density and size estimates for spiral galaxies using General Relativity. Astrophys Space Sci. **362**, 210–231 (2017)
20. D. Astesiano, S.L. Cacciatori, V. Gorini, F. Re, Towards a full general relativistic approach to galaxies. Eur. Phys. J. C **82**, 554 (2022)
21. D. Astesiano, M.L. Ruggiero, Galactic dark matter effects from purely geometrical aspects of General Relativity. arXiv:2205.03091v1 [gr-qc] (2022)
22. C. Corda, Interferometric detection of gravitational waves: the definitive test for General Relativity. Int. J. Mod. Phys. D **18**, 2275–2282 (2009)
23. G.O. Ludwig, Galactic rotation curve and dark matter according to gravitoelectromagnetism. Eur. Phys. J. C **81**, 186 (2021)
24. G.O. Ludwig, Extended gravitoelectromagnetism. I. Variational formulation. Eur. Phys. J. Plus **136**, 373 (2021)
25. G.O. Ludwig, Extended gravitoelectromagnetism. II. Metric perturbation. Eur. Phys. J. Plus **136**, 465 (2021)
26. Y. Srivastava, G. Immirzi, J. Swain, O. Panella, S. Pacetti, General Relativity versus dark matter for rotating galaxies. Eur. Phys. J. C **83**, 100 (2023)
27. O. Heaviside, A gravitational and electromagnetic analogy, in *Electromagnetic Theory*, vol. I, (The Electrician, London, 1893), pp.455–466
28. M.L. Ruggiero, A. Ortolani, C.C. Speake, Galactic dynamics in General Relativity: the role of gravitomagnetism. arXiv:2112.08290 [gr-qc] (2021)
29. D. Astesiano, M.L. Ruggiero, Can General Relativity play a role in galactic dynamics? arXiv:2211.11815v1 [gr-qc] (2022)
30. M.L. Ruggiero, A note on the gravitoelectromagnetic analogy. arXiv:2111.09008v1 [gr-qc] (2021)
31. G.O. Ludwig, Sedimentation equilibrium of globular and galaxy clusters. Int. J. Mod. Phys. A **38**, 2342001 (50pp) (2023)
32. S. Chandrasekhar, *An Introduction to the Study of Stellar Structure* (Dover Publications, Inc., New York, 1958)
33. S.L. Shapiro, S.A. Teukolsky, *Black-Holes, White Dwarfs, and Neutron Stars—The Physics of Compact Objects* (Wiley-VCH, Weinheim, 2004)
34. I. Sagert, M. Hempel, C. Greiner, J. Schaffner-Bielich, Compact stars for undergraduates. arXiv:astro-ph/0506417 (2005)
35. S.P. Weppner, J.P. McKelvey, K.D. Thielen, A.K. Zielinski, A variable polytrope index applied to planet and material models. arXiv:astro-ph.EP/1409.5525v2 (2015)
36. H.C. Plummer, The distribution of stars in globular clusters. Mon. Not. R. Astron. Soc. **76**, 107–121 (1915)
37. G.O. Ludwig, Larmor rotation in galaxies. Eur. Phys. J. C **82**, 281 (2022)
38. V.D. Shafranov, L.E. Zakharov, Use of the virtual-casing principle in calculating the containing magnetic field in toroidal plasma systems. Nucl. Fusion **12**, 599–601 (1972)
39. K. Lackner, Computation of ideal MHD equilibria. Comput. Phys. Comm. **12**, 33–44 (1976)
40. R.A. James, The solution of Poisson's equation for isolated source distributions. J. Comput. Phys. **25**, 71–93 (1977)
41. R.A. James, Techniques for simulating galactic collisions. in: Investigating the Universe. Papers Presented to Zdeněk Kopal on the Occasion of his Retirement, September 1981, ed. by F.D. Kahn. Astrophysics and Space Science Library, vol. 91 (D. Reidel, Dordrecht, 1981), pp. 423–441
42. S. Jardin, *Computational Methods in Plasma Physics* (CRC Press, Boca Raton, FL, 2010)
43. J.D. Hanson, The virtual-casing principle and Helmholtz's theorem. Plasma Phys. Control. Fusion **57**, 115006+4 (2015)
44. W. Israel, Singular hypersurfaces and thin shells in General Relativity. Nuovo Cimento B **44**, 1–14 (1966)
45. L. Woltjer, A theorem on force-free magnetic fields. Proc. Natl. Acad. Sci. USA **44**, 489–491 (1958)
46. G.O. Ludwig, Analytic solution of the tokamak equilibrium. I. The fixed-boundary case. Phys. Plasmas **24**, 092502 (2017)
47. G.O. Ludwig, Analytic solution of the tokamak equilibrium. II. The free-boundary case. Phys. Plasmas **24**, 092503 (2017)
48. S.P. Drake, R. Turolla, The application of the Newman–Janis algorithm in obtaining interior solutions of the Kerr metric. Class. Quantum Gravity **14**, 1883–1897 (1997)

49. S.P. Drake, P. Szekeres, Uniqueness of the Newman–Janis algorithm in generating the Kerr–Newman metric. Gen. Relat. Gravit. **32**, 445–457 (2000)
50. R.P. Kerr, Do black holes have singularities? https://www.researchgate.net/publication/375744216 (2023)
51. E. Oepik, An estimate of the distance of the Andromeda nebula. ApJ **55**, 406–410 (1922)
52. R.B. Tully, J.R. Fisher, A new method of determining distance to galaxies. Astron. Astrophys. **54**, 661–673 (1977)
53. D. Saadeh, S.M. Feeney, A. Pontzen, H.V. Peiris, J.D. McEwen, How isotropic is the universe? Phys. Rev. Lett. **117**, 131302-1–131302-5 (2016)
54. P. Brosche, Über das Masse-Drehimpuls-Diagramm von Spiralneben und anderen Objekten. Z. Astrophys. **57**, 143–155 (1963)
55. V. Trimble, Angular momentum versus mass, re-examined. Comments Ap. **10**, 127–135 (1984)
56. S.S. McGaugh, J.M. Schombert, G.D. Bothun, J.G. de Blok, The baryonic Tully–Fisher relation. ApJ **533**, L99–L102 (2000)
57. R.B. Tully, H. Courtois, Y. Hoffman, D. Pomarède, The Laniakea supercluster of galaxies. Nature **513**, 71–73 (2014)
58. J.H. Oort, Observational evidence confirming Linblad's hypothesis of a rotation of the galactic system. Bull. Astron. Inst. Neth. **3**, 275–282 (1927)